Università degli Studi di Padova

DIPARTIMENTO DI INGEGNERIA INDUSTRIALE
Corso di Laurea Magistrale in Ingegneria dell' Energia Elettrica

Tesi di laurea magistrale

Modelling and power-voltage control in unbalanced bipolar multi-terminal HVDC grids

Studente:
Chiara Berto
Matricola 1081871

Docente:
Prof. Roberto Benato

Correlatore:
Prof. Dirk Van Hertem

Anno Accademico 2015/2016

Contents

Abstract

The energy sector in the European Union is experiencing a substantial change since the last few decades. The scientific community and public concern on global warming motivated the European authorities to set ambitious targets, in order to invert the increasing trend of temperature and Green House Gasses concentration in the atmosphere.

The decarbonization of electricity production gives a major contribution to the achievement of these targets. Hence, CO2 free technologies have to be implemented for the energy generation. Therefore, the European Union has been promoting the integration of power plants from renewable sources in the network.

As a consequence, the transmission power system is facing the need to became more flexible in order to handle the energy from renewable sources as wind and solar that are for their nature variable and unpredictable. Furthermore, renewables are often concentrated in remote locations, in the North of Europe for wind and in the South for solar. The transmission grid has to cover long distances and the traditional alternating current technology is not well suited for this task.

High-Voltage Direct-Current (HVDC) transmission has already been used to connect offshore wind plants with the mainland and as interconnction of asynchronous zones, but this technology is potentially suited for a reinforcement of the entire European network. An HVDC system could increase the number of interconnections making the energy supply more efficient and reliable, and the energy market more competitive. In this sense, the concept of a pan-European Supergrid has been introduced and research is spending a lot of efforts in the study of the management of such a system, identifying the Voltage Source Converter technology as the best solution for a meshed multi-terminal HVDC grid.

This thesis wants to give a contribution on the analysis of multi-terminal meshed VSC-HVDC grids. In particular the possible configurations are described and the main focus is given to the modeling and control of a meshed bipolar system. The distributed voltage control strategy, called droop control, is investigated and simulations are performed to evaluate the dynamic behavior of the voltage regulator after the outage of a converter. In particular the consequences of an asymmetric converter outage in the bipolar configuration are studied. Finally, the influence of grid parameters as return path resistance, lines length and droop gain on the coupling between the two poles is mathematically described.

Sommario

Negli ultimi decenni il settore energetico sta fronteggiando sostanziali cambiamenti. Le autorità europee, in risposta agli avvertimenti della comunità scientifica e alla crescente preoccupazione dell'opinione pubblica riguardo al riscaldamento globale, hanno stabilito degli ambiziosi obiettivi con la finalità di invertire la tendenza all'aumento della temperatura media superficiale e della concentrazione di gas serra in atmosfera.

La decarbonizzazione dei processi di produzione di energia elettrica d un contributo fondamentale al raggiugimento di tali obiettivi. Per questo motivo sono state introdotte tecnologie di generazione ad emissione nulla di anidride carbonica (CO2), di cui l'Unione Europea (UE) ha facilitato l'inserimento nel quadro di produzione, promuovendo incentivi allo sviluppo degli impianti di generazione di energia elettrica da fonti rinnovabili.

Di conseguenza il sistema elettrico di trasmissione si trova a fronteggiare la necessità di acquisire una maggiore flessibilità, in modo da riuscire a gestire l'energia prodotta dalle fonti rinnovabili, come l'energia eolica e l'energia solare, le quali sono per loro natura variabili e non prevedibili. Inoltre, le fonti rinnovabili sono spesso concentrate in località remote rispetto alla rete industriale di trasmissione e ai carichi, nello specifico nel Nord Europa per l'eolico e nel Sud Europa per il solare. Perciò, le distanze che le linee di trasmissione devono coprire sono consistenti e il tradizionale sistema in corrente alternata presenta svantaggi tali da non essere conveniente per assolvere il compito di trasmettere l'energia ai carichi.

Il sistema di trasmissione ad alta tensione e corrente continua (HVDC) è già stato usato in passato in vari modi, come connettere gli impianti eolici off-shore con la terraferma ed interconnettere zone della rete non sincrone. Questa tecnologia è anche potenzialmente adatta per rinforzare l'intero sistema elettrico europeo. Una rete HVDC potrebbe aumentare il numero delle interconnessioni tra diverse nazioni rendendo la fornitura di energia elettrica pi efficiente ed affidabile e il mercato più competitivo. In questo senso, il concetto di una "super-grid" paneuropea è stato introdotto e la ricerca sta investendo molte risorse nello studio della gestione e del controllo di una tale rete, identificado nella tecnologia dei converter a tensione impressa (Voltage Source Converters, VSC) la soluzione migliore per una rete HVDC multi-terminale e magliata.

Questa tesi vuole dare un contributo all'analisi dei sistemi multi-terminale VSC-HVDC. Sono innanzitutto descritti i vantaggi della trasmissione a corrente continua rispetto alla corrente alternata e i vantaggi della conversione a tensione impressa rispetto alla conversione a corrente impressa. Sono poi elencate le differenti configurazioni, monopolare o bipolare, simmetrica o asimmetrica, con cui pu essere progettato il sistema HVDC, accennando quindi al tema dell'estensibilità di una linea in una vera e propria rete tramite la connessione progressiva con altre linee. Segue poi l'accurata descrizione della modellazione e del controllo dei sistemi bipolari magliati. La strategia di controllo distribuito, chiamata "droop control", è investigata e tramite simulazioni Simulink è valutato il comportamento dinamico del regolatore di tensione in seguito al fuori servizio di uno dei convertitori della rete. In particolare, sono studiate le conseguenze di un fuori servizio asimmetrico, cioè di un convertitore appartenente ad un terminale e di una singola polarità. Infine, è matematicamente descritta l'influenza dei parametri di rete, quali resistenza del percorso di richiusura della corrente, lunghezza delle linee e guadagno di droop, sull'accoppiamento tra i poli del sistema bipolare. L'accoppiamento è definito come il grado di reazione con cui un polo compensa lo sbilanciamento causato da una contingenza sul polo opposto.

List of Abbreviations and Symbols

Abbreviations

AC	Alternating Current
AWU	Anti Wind Up
CO2	Carbon Dioxide
CSC	Current Source Converter
DC	Direct Current
EU	European Union
GHG	Green House Gas
HVAC	High-Voltage Alternating-Current
HVDC	High-Voltage Direct-Current
IGBT	Insulated Gate Bipolar Thyristor
IGCT	Integrated Gate Commutated Thyristor
LCC	Line Commutated Converter
MI	Mass Impregnated
MMC	Modular Multilevel Converter
MTDC	Multi-Terminal Direct-Current
OPF	Optimal Power Flow
OPWM	Optimal PWM
PCC	Point of Common Coupling
PI	Proportional Integral
PISA	Piemonte-Savoie VSC-HVDC line
PLL	Phase Locked Loop
PWM	Pulse Width Modulation
RTE	Réseau de Transport dÉlectricité, French system operator
SHEM	Selective Harmonic Elimination Modulation
SVD	Singular Value Decomposition
TERNA	Italian system operator
TSO	Transmission System Operator
VSC	Voltage Source Converter
XLPE	Cross-Linked PolyEthylene

Symbols

C_C	Converter DC capacitance
C_{DC}	DC branch capacitance
c_{DC}	DC branch capacitance per length
dq	Synchronously rotating reference frame
e	Error
g_{DC}	Converter droop gain
G	Diagonal matrix of the converters gains
I_C	DC capacitance current
I_{DC}	DC current
I_L	DC line current
I_s	AC side current phasor
k_{DC}	DC droop constant
k_i	Current controller integral gain
k_{ip}	Active power controller integral gain
k_{pp}	Active power controller proportional gain
k_p	Current controller proportional gain
l	Line length
L_s	AC side inductance
L_{DC}	DC branch inductance
P_{DC}	DC power
P_s	VSC AC side active power
Q_s	VSC AC side reactive power
R_s	AC side resistance
R_{DC}	DC branch resistance
R_{dcm}	Metallic return resistance
t	Time
U_{DC}	DC voltage
U_c	Converter AC side voltage
U_s	AC grid voltage
x	Line length
$\mathsf{Y_{DC}}$	DC bus admittance matrix
$\underline{Z}_s$	complex AC side impedance
δ	Phasor angle
Δ	Deviation
pi	DC cable model
φ	Phasor angle
τ_C	Time constant of the DC capacitor
τ_i	Current control loop time constant
ω	Grid pulsation

Chapter 1

Introduction

1.1 Context and motivation

The energy sector has been facing multiple challenges since the last couple of decades and more important are the changing foreseen in the next few years. The severe increase of Green House Gases (GHG) in the atmosphere is followed by a rise of the global surface temperature. The two trends can be seen in figure 1.1 (a) and (b).

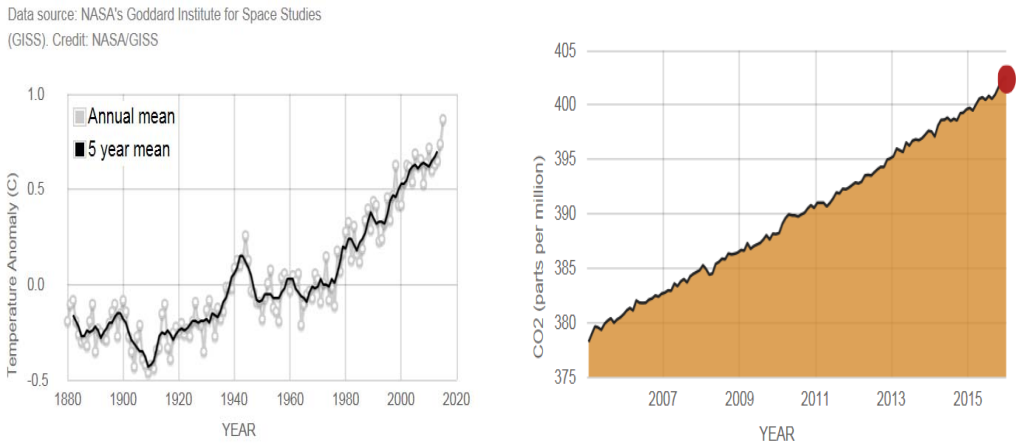

(a) Change in global surface temperature relative to 1951-1980 average temperatures [1].

(b) Green House Gases concentration in the atmosphere [1].

Figure 1.1: Global surface temperature and greenhouse gas concentration

Since the increase of the surface temperature is a concern for the health of the planet, a big interest is now being directed towards those energy sources that are CO2 free. European authorities have developed a plan called the 20-20-20 agreement, which was approved in 2008 and sets three targets that have to be achieved before 2020. The agreement aims at reducing the GHG emissions by 20%, at increasing the efficiency by 20% and at reaching a 20% share of energy production by renewable sources [2]. In 2014 a follow-up agreement has been approved, which gives the targets that the European Union (EU) has to reach in the period 2020-2030 [3]. Finally a study called *"Roadmap 2050: a practical guide to a prosperous, low-carbon Europe"* investigates the technical and economic feasibility of achieving at least an 80% reduction in greenhouse gases emissions by 2050 with respect to 1990 levels. The report, commissioned by the leaders of the EU, analyzes the technical and economical achievability of a GHG reduction while maintaining or improving the actual levels of energy security, economical growth and prosperity. Furthermore it investigates the consequences of the required actions on the European energy sector over the next 5 to 10 years [4].

In this context many governments have supported the development of renewable sources in their countries which resulted in a differentiated generation mix. Figure 1.2 shows the share of new power capacity installations in EU in the last year. It is noticeable that wind power was the technology with the highest installation, accounting for 44% of the total, followed by solar with 29%. In total, renewables cover the 77% of the new capacity installed in 2015. Figure 1.3 shows the comparison between the European power mix in 2000 and after 15 years. Over this period of time, the share in the total installed power capacity has grown from 24% to 44% [5].

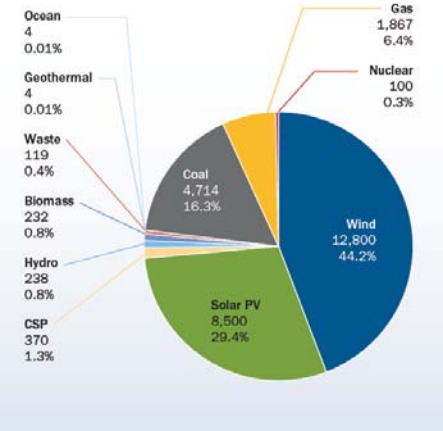

Figure 1.2: Share of new power capacity installations in EU in 2015 [5]

On one hand the study *"Roadmap 2050"* confirmed that the 80% reduction of GHG by 2050 is achievable only with a 95 to 100% decarbonized power sector, on the other hand the integration of renewable sources gives rise to multiple challenges from the point of view of the management of the electrical infrastructure and the planning of the generation. Technologies collecting energy from wind or sun are dependent on external factors as weather or location, they are variable and unpredictable. The first issue is to connect the remote locations where wind farms or solar plants are profitable to the more centralized load system [6]. The actual grid, already heavily charged, is experiencing severe congestion because of the long distance transmission required by the renewable generation. The second issue is to provide the capacity needed to cope with the variability of renewable sources generation. The corresponding grid reinforcement that results from the integration of renewable sources, is also a priority identified by the EU. In particular the *"Communication from the commission to the European parliament and the council"* dated February 2015 sets the goal of a 10% electricity interconnection target (updated to 16 %) [7]. A more interconnected European grid creates competition between national markets, resulting in a lower price of the electric energy. Besides, it also ensures a more secure and sustainable energy. The actual situation of import dependency, outdated infrastructure and lack of investment, has to be improved if the European Union wants to guarantee a low-carbon energy sector and an effective action against the climate change.

To overcome the issues that electricity generation from renewable sources is causing to the grid, in [8][6][9][10] an European supergrid has been discussed. Wind generation in the North European countries can be connected to solar energy in the south of Europe or even in the Saharan region to reduce the variability, since their dependence on weather is poorly correlated; the rest could be balanced with hydro energy or even geothermal energy largely present in Iceland [6]. A pan-European supergrid would also improve the security of supply, balance the network and enhance the market both on European and global scale. In fact, a free continental market of the electrical energy could be created, increasing the competition. Furthermore companies could export the technology to the other continents. To build this supergrid, High-Voltage Direct-Current (HVDC) technology is identified as the preferred solution due to the advantages it presents over HVAC (High-Voltage Alternate-Current) transmission in terms of losses and acceptability from the public. For these reasons, the research on HVDC is extending from the simple two terminals configuration to a multi-terminal and meshed grid layout, analyzing and

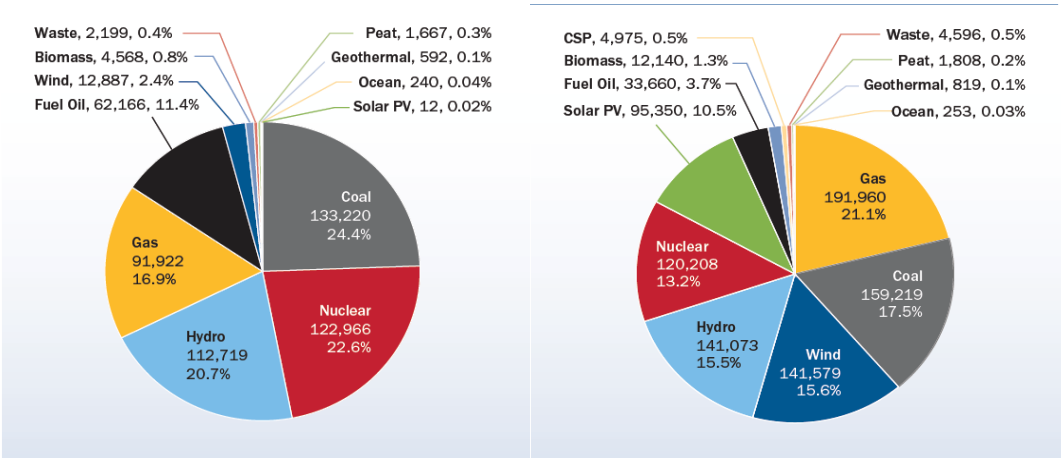

(a) EU power mix 2000 (MW) [5]

(b) EU power mix 2015 (MW) [5]

Figure 1.3: European power mix share. Comparison between the year 2000 and the year 2015.

solving all the possible issues for the control and operation of such a grid and its integration in the existing AC grid.

1.2 Contribution of the thesis

This thesis provides a contribution to the study of meshed multi-terminal HVDC grids. In particular the analysis focuses on the voltage stability of a droop controlled bipolar VSC-HVDC configuration when it is facing the outage of a converter. The impact of the outage on the opposite pole is studied and a methodology to evaluate the influence of the grid parameters on the size of the imbalance is developed. Results are supported by dynamic simulations performed on a model of the grid built in MATLAB Simulink.

Chapters two describes the converter technologies adopted in a HVDC grid, focusing more on the voltage source converter. Furthermore the advantages of HVDC transmission over AC transmission are given. Chapter three contains an overview on the possible configurations of the VSC-HVDC grid. Insights on the network extensibility and grounding are also given. In chapter four the voltage control strategies (centralized and distributed) are investigated and applied on a three terminals monopolar network in order to prove their working principle. Chapter five describes the modelling of a bipolar multi-terminal HVDC grid with the aim of investigating the dynamic behavior of the controllers in the two poles. Simulations are performed on a four terminals bipolar network to understand if a stable operative point is reached after the outage of a converter in one of the poles. Finally, the coupling between the two poles of a bipolar configuration is analyzed in chapter six. The term coupling has to be intended as the degree of reaction of a pole after a contingency in the other pole. The reaction is measured with voltage and power variation at the grid terminals. The influence of the grid parameters (as metallic return resistance, lines length and droop gain) on the coupling is shown.

Chapter 2

VSC-HVDC multi-terminal grid

2.1 Historical background

HVDC is not a new technology. The first experiments with electricity were based on direct current (basic discoveries of Galvani, Volta, Oesterd, Ohm and Ampére) [11]. At the end of the nineteenth century, thanks to the support of the Thomas Edison's company, the direct current power system was considered for the distribution and the transmission of electrical energy as well as the alternating current system. However, the invention of the transformer, the polyphase circuit and the induction motor gave the AC power system a definitive advantage. In fact transformers enable to change the voltage level to a value suited for long distance-high voltage transmission. In the beginning, when the AC power system was preferred, converter technology was not developed yet and direct current transmission had strict limits on voltage and current. The scientific community never forgot the advantages DC transmission has over AC transmission and the study of its practical application gained popularity in the 1950's, when mercury-arc valves became commercially available. Thanks to the progress in the area of power electronics, mercury-arc valves were replaced by switching devices like thyristors and later IGBTs. The AC/DC conversion increased substantially its power ratings allowing the realization of DC transmission links dimensioned for up to 7.2 GW.

2.2 Advantages of HVDC over AC transmission

The interest in HVDC transmission is justified by the advantages this system has over AC transmission. Even if it is not expected that the AC system will be completely replaced by a DC system, the convenience of the last makes it the better choice in view of a reinforcement of the grid. In fact as we said in the introductory chapter, the European grid is facing the necessity of a radical change. The future grid has to be able to integrate up to 80-100% of generation from renewable sources, that are by their very nature variable and unpredictable. Those sources are widely available in remote locations, for example offshore wind farms in the northern European seas. Thus a long distance has to be covered to connect them to the rest of the grid. This has to be done in a manner that takes into account the increasing opposition of the public society to the building of new ahead lines. The DC transmission system can be the solution to these issues. The advantages that it has over the AC system are:

Investment costs. Even if the initial cost of the DC converter station in very high, the total investment for a long transmission DC system is lower then for an AC system. This is due to the fact that the number of conductors required in an AC line are three, in a DC line two conductors are necessary, only one in the case of a monopolar configuration with ground return. Therefore, if for a short link the DC system is not convenient, there is a certain transmission distance (break-even distance) from which the overall investement becomes lower for the DC system then the AC system.

Cable connections. In HVDC transmission there is no charging current in steady-state con-

dition. For this reason the use of cables is easier compared to AC transmission. In the last one the charging current is present and since it is directly dependent on the voltage level and on the lines capacitance value, it can be preponderant, not allowing the cable to transport any active power. Furthermore, to obtain the approval for the building of a new overhead line is becoming very challenging as the public society is concerned of the environmental consequences of it. New underground cable links usually do not suffer from this opposition. Finally, undersea cables are the only feasible way to connect off-shore wind farms with the mainland.

Losses and long distance transmission. When an alternating current is flowing in a conductor, the physical phenomenon called "skin effect" arises. Because of this effect, the distribution of the current over the conductor section is not homogeneous and the current density is higher near the surface. This skin effect causes the resistance of the conductor to increase, reducing its effective cross-section. In DC transmission the phenomenon is absent and all current attributes to the active power transmission. Hence, the losses in DC systems are lower compared to an AC system with the same ratings. Long distance is problematic for AC lines also because of subsynchronous resonances. This phenomena occurs when a resonant frequency of turbine generators shafts coincides with a natural resonant frequency of the power system. Such resonances can lead to serious damages like shaft failure.

Asynchronous interconnections. HVDC lines can link two or more asynchronous AC systems that are operating at the same or at a different frequency.

Improved controllability. The power flowing through the DC line is fully controllable, making the link available for ancillary services like sharing of primary reserves or power system damping.

Firewall for AC faults. A DC link can be a division between two systems when one of them is experiencing a fault. The DC link can avoid the fault to propagate into the other system.

2.3 Multi-terminal grid development

How the layout of the future interconnected European grid will look like is still not certain. A 150 billion investment is planned to reinforce the actual grid by 2050 [12] and for sure HVDC links will play an important role in this development. As it is reported in the list of projects under construction and under planning [13], the number of two terminals HVDC links is increasing. These new links will appear for different purposes: to connect off-shore wind farms to the mainland, to increase the power trade between different countries, as interconnectors between wind solar and hydro resources and to integrate energy storage in the grid and to connect asynchronous AC systems [14]. It is not clear yet if these HVDC links will remain independent end-to-end systems or if they will be connected to create a real meshed grid. A meshed grid requires an advanced control system that has to take into account the interactions with the AC grid, but when an optimal operation of the combined system is found, the solution of a meshed DC grid brings important advantages. For example, a meshed layout increases the reliability of the system. The risk that a part of the grid or a functioning generation plant are isolated because of a line outage is in this way eliminated. Other advantages for the whole system are that meshed connections increase transmission capacity while reducing dimensioning ratings of the grid components, in fact since the peaks of demand of different AC load systems do not occur at the same moment in time, the sum of the peaks of multiple point to point links is higher than the peak of demand of a meshed grid. In this way the power capacity of the single component of the grid is reduced, which reduces their price as well. Furthermore, for a meshed grid the maintenance of the converter stations is easier since there are more possibilities to reroute the power to other converters [15]. Also the integration of renewable sources is more effective as for example, the meshed grid being connected to a more differentiated and flexible load, allows a reduction of the energy curtailments from wind farms [15]. Figure 2.1 shows a

vision about how a future north European off-shore meshed grid (also called supergrid) may look like.

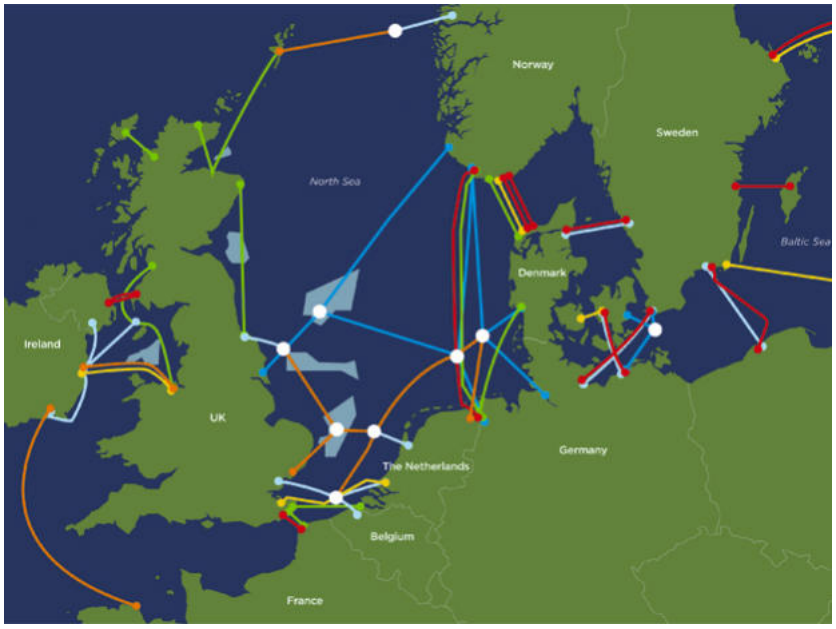

Figure 2.1: Vision of the European off-shore meshed grid [16].

2.4 VSC versus CSC

The HVDC grid analysed in the following chapters of this thesis is a multi-terminal meshed grid. At every terminal of the grid there is a converter station and in every station there is a single converter (if the grid is monopolar), or two converters (if the grid is bipolar). The converters are Voltage Source Converters (VSC). They have been chosen because they appear as the most advantageous technology for multi-terminal and meshed HVDC grids [6]. VSC became available relatively recently, in the 90's. Before this data, the available converters were the Current Source Converters (CSC), also called Line-Commutated Converters (LCC). The majority of the existing HVDC transmission lines implements the conventional CSC technology, but an increase of the use of VSC technology is expected in the future.

2.4.1 CSC-HVDC technology

Current Source Converters are devices that consist of thyristor valves as switching components. Thyristors took the place of mercury arc valves, ionic rectifiers with the disadvantage of being subjected to arc-back faults when submitted to a high reverse voltage [17]. Thyristors do not have the arc-back fault problem and nowadays they reach significant ratings of voltage and current, i.e. up to 8,5 kV as blocking voltage and 6,1 kA as current rating with expectancy of improvement in the next years [18].

Thyristors have controlled ignition but they need to await a current zero crossing to switch off. For this reason, they depend on an external AC voltage source for the commutation process. In figure 2.2 (a) the thyristor bridge connected to the line is shown. It has an inductance L at the DC side that is responsible for the reduction of the DC current harmonics. Hence, the CSC operates with a constant DC current. The power reversal in such a converter is done by changing the polarity of the voltage. In fact the voltage can be controlled thanks to the variation of the firing angle of the thyristors. When the firing angle is higher than 90 degrees of the commutation period, the voltage becomes on average negative.

Since it is not possible to command the switching off of thyristor valves, CSC need a strong synchronous voltage source to operate. The three-phase symmetrical short circuit capacity

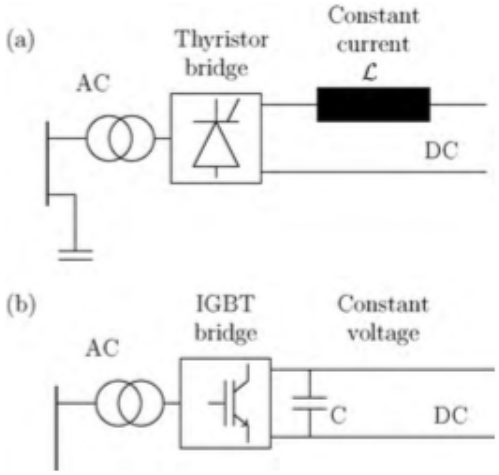

Figure 2.2: CSC and VSC-HVDC one line diagram. (a)Current Source Converter, (b)Voltage Source Converter [6]

available from the network at the converter connection point should be at least twice the converter rating [19]. For this reason, they are not suitable to convert the power coming from weak islanded sources like offshore wind farms. Furthermore these converters operate with the AC current lagging the voltage, as consequence of the commutation from one phase to another and as a consequence of the firing angle of the thyristors. Hence, they absorb reactive power up to 50-60% of the power rating. The reactive power is generally delivered through switchable capacitor banks, harmonic filters, Static Var Compensator (SVC), a generator or a synchronous condenser.

A problem that CSCs can manifest is commutation failure. This problem occurs when the commutation from one phase to another is missed because the voltage reverses before the current zero crossing. The DC side experiences a short circuit and the power exchanged goes to zero for that commutation period. These failures are more frequent in inverter mode, or when the external grid has low voltage or when the DC side has a high current operation point. When the number of the failures is substantial, the entire HVDC link may be forced to trip [20].

2.4.2 VSC-HVDC technology

Because of the previous drawbacks of CSC for MTDC transmission, the interest for VSC increased, even if CSC-HVDC transmission is a mature technology and it is generally cheaper than VSC-HVDC transmission. Voltage Source Converters are classified as *self-commutated converters* because they are made of switches able to be controlled in terms of both ignition and shutdown. Contrary to CSC that have a constant current at the DC side, VSC delivers a constant voltage as is depicted in figure 2.2(b). Its online schematic consist in a switches group with a parallel capacitor. In this type of device the conversion of polarity occurs when the current changes its sign. For this reason, a VSC requires switches, capable of conducting both positive and negative current; e.g. the switch cells of Insulated Gate Bipolar Transistor (IGBT) or the reverse conducting Integrated Gate-Commutated Thyristor (IGCT) or the antiparallel connection of a Gate Turn-Off Thyristor (GTO) and a diode. Nowadays IGBTs are predominant and there are commercially available devices with voltages up to 6,5 kV and current ratings of 3,6 kA [18]. VSC-HVDC links with DC voltage ratings of $\pm$525 kV and power up to 3 GW are being projected [13]. Having a fixed DC voltage polarity, VSC-HVDC transmission has an important advantage over CSC-HVDC where the voltage is reversed to change the power direction. Therefore, it is possible to use polymeric (e.g. crosslinked polyetilene XLPE) cables instead of the more expensive and difficult to use, Mass-Impregnated cables (MI).

Voltage Source Converters can be built in a so called two-levels topology, in a multi-level

topology or in a multi-modular one. In a two- or three-level topology, the voltage is synthesized with the Pulse Width Modulation technique (PWM) varying the output voltage between the negative DC value and the positive one (in case of a two levels converter) or between negative, zero and positive DC voltage (in case of a three-level converter). The resulting voltage is shown in figure 2.3 (a) for the two levels, (b) for the three levels. The downside of the two and three-level topology is the high losses, up to 3% and 1.7% respectively [21]. For the multi-level topology other techniques, e.g. the Selective Harmonic Elimination Modulation (SHEM) or the optimal PWM (OPWM), were developed to modulate the voltage at the fundamental frequency in order to reduce the harmonic content and to lower the switching losses [22].

In the case of a Multi-Modular Converter (MMC), the resulting voltage is synthesized in a step manner, as shown in figure 2.3(c), it does not contain high frequency harmonics and the losses are reduced to about 1% per converter station [21].

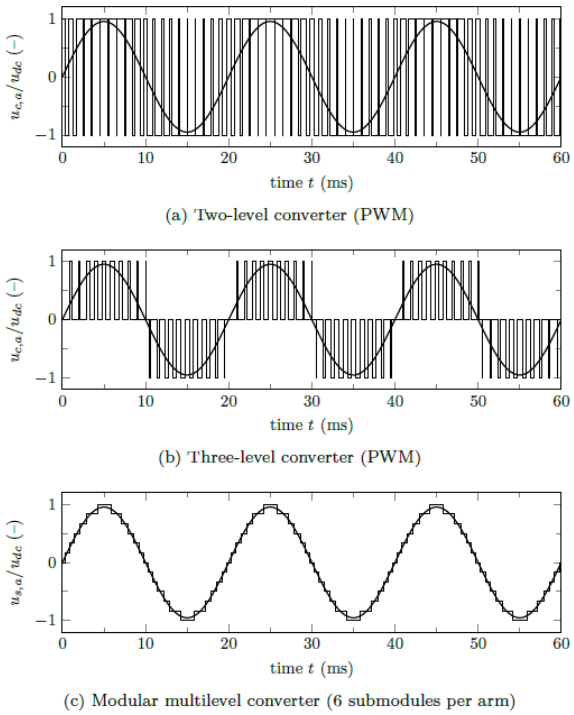

Figure 2.3: Switching pattern for different converter topologies [21].

Losses are higher when the switching frequency increases. With the multi-modular topology it is possible to achieve lower losses because the switching frequency per valve is substantially lower [23]. The MMC scheme is shown in figure 2.4. Multiple submodules are cascaded in every converter arm and, unlike the other topologies, a common DC capacitance is not present. The submodules are the basic components, when their number increases also the number of levels available to synthesize the desired voltage increases.

In figure 2.5 two possible submodule configurations are shown; (a) is a half bridge scheme, (b) is a full bridge scheme [24]. The number of switches in the full bridge scheme is double compared to the half bridge, but the first one can block the current flowing in both directions. Thus, contrarily to the half bridge submodule, it can block DC fault currents.

A strong external voltage wave is not needed for the correct operation of a Voltage Source Converters. In fact, the switches in this technology do not need a zero current crossing for the commutation. This aspect gives another advantage to VSC-HVDC because it can be used to connect weak systems (e.g. off-shore wind farms) or even for a black start. Furthermore Current Source Converters consume reactive power due to the lagging of the current caused by the thyristors firing angle; on the contrary Voltage Source Converters can independently control the active and reactive power. The full controllability of the power in the VSC technology makes

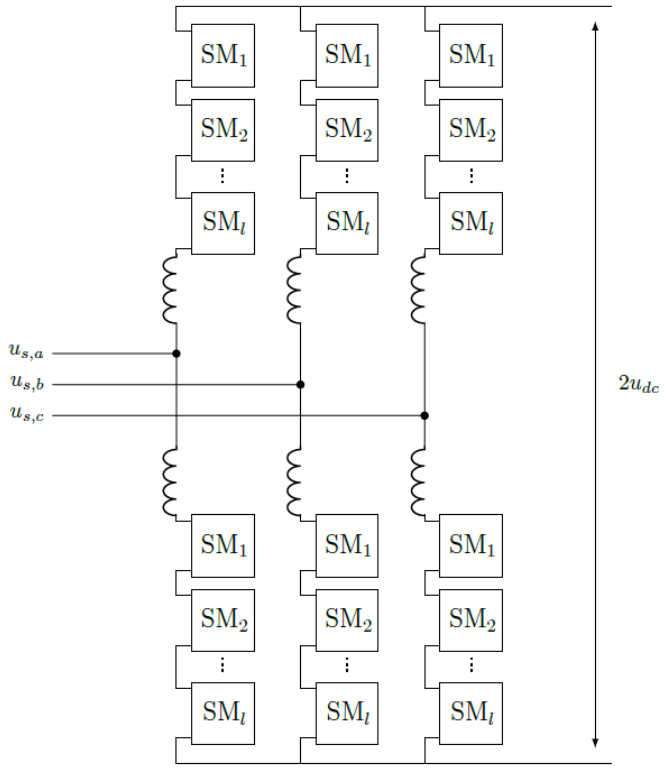

Figure 2.4: Multi modular converter topology [21].

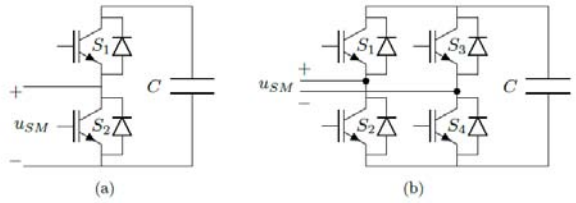

Figure 2.5: MMC basic component model. (a) Half bridge, (b) full bridge [21].

it also suited for ancillary services. Compared to CSCs the only drawbacks of VSCs are: higher losses due to a higher switching frequency, lower power rating because of the actual technological limits of IGBTs and a lower expertise in their use in HVDC transmission lines.

It is reasonable to expect that a future meshed grid will use the VSC technology as it has a common DC voltage that makes easier to control and to extend the grid connecting parallel systems. In addition, if CSC are used in a meshed grid, the power reversal in a particular branch is done through the change of voltage polarity, this could affect the power direction also in other branches. Finally, VSC-HVDC converters can connect weak and islanded grids to the centralized system.

2.5 An example: the Piemonte-Savoie VSC-HVDC line

The use of the VSC-HVDC technology as an interconnector between countries and as a strenghtening of the entire network, can be well exemplified by the Piemonte-Savoie line, also called PISA.

It is one of the VSC-HVDC projects currently under construction, a two-terminal line connecting Italy and France, a collaboration between the Italian system operator TERNA and the French RTE. The realisation of the link, approved in 2011, started in 2013 in the Italian territory and in 2015 in the French side [25]. Finally, commissioning is scheduled for 2019. At the moment of writing, the installed capacity of interconnection between Italy and France is 2650 MW. The energy exchange is done mainly through the 400 kV AC lines Albertville-Rondissone and Albertville-Venaus. However, the current capacity is for most of the time saturated. This is one of the reasons why it has been decided to build a new interconnection. The advantages of new "Piemonte-Savoie" line are:

- to increase the capacity of mutual aid between Italy and France,
- to improve the sharing of resources between the two countries,
- to facilitate cross-border exchanges of electric energy,
- to facilitate the integration of renewable sources in the Italian and French electricity grids [26].

The two-terminal HVDC link connects the electric stations of Piossasco, near Turin and Grand-ÎIle in Savoie. It consists of an extruded underground cable, with crosslinked polyethylene insulation (XLPE) following a 190 kilometers long route, approximately 95 kilometers in each country [27] (figures 2.6 and 2.7 show the route). For its length, its voltage level (±320

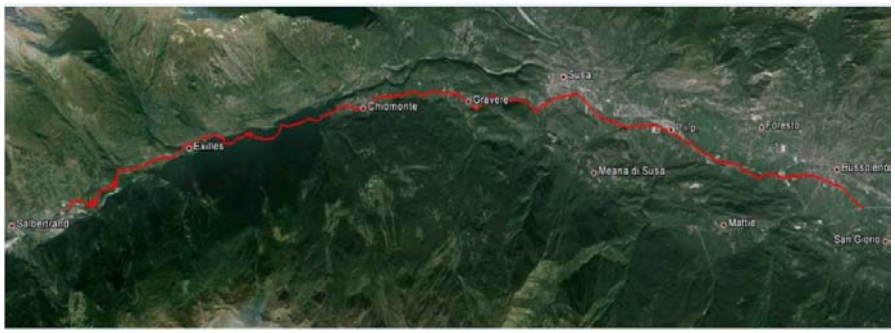

Figure 2.6: Route of the HVDC line in Italy [25].

kV) and for being an underground line, the Piemonte-Savoie project is the first of its kind in the world [26]. The realization of the conversion stations has been assigned to the French company Alstom. Alstom will design, manufacture and commission two converter stations ($2 * 600$ MW, ±320 kV) containing Alstoms Voltage Source Converter technology [28]. The VSC technology has the advantage of offering a high rate of reversal of the current (50 milliseconds), which

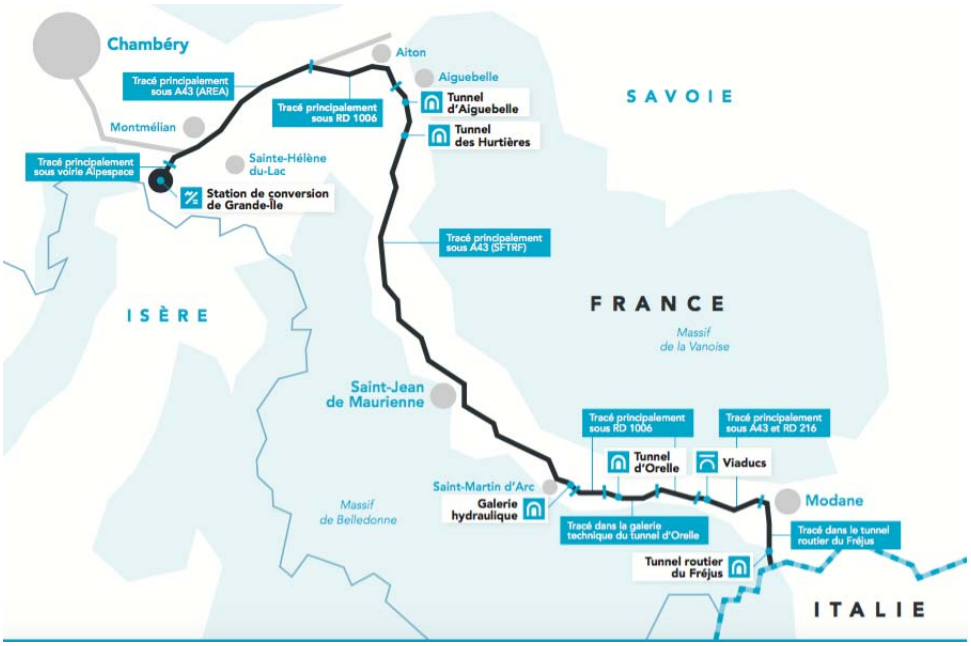

Figure 2.7: Route of the HVDC line in Frace [26].

allows great flexibility in the management of exchanges with Italy and precise adjustment of the voltage level. Furthermore, it guarantees security of supply and electrical quality. VSCs are more compact than the older technology of controlled converters (LCCs using thyristors), as a consequence, VSCs allow to halve the size of facilities, giving a significant advantage in terms of environmental impact [26]. The environmental impact of the entire project is minimal also due to the fact that the cables will be installed under the existing road infrastructures using four polyethylene sleeves arranged in a square at the bottom of a trench, and crossing the border in the Frejus safety tunnel. Figure 2.8 shows the cables layout. The chosen HVDC configuration

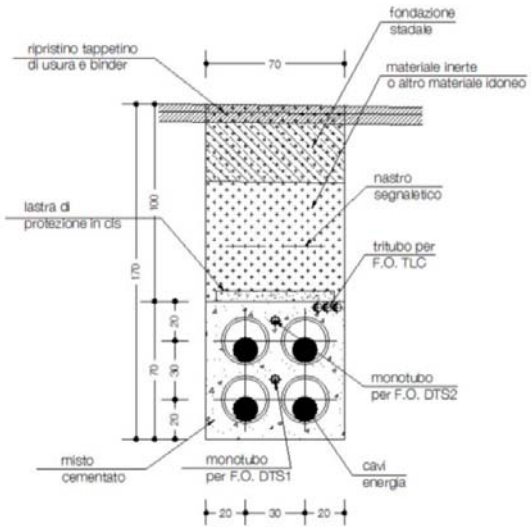

Figure 2.8: Underground trench to allocate the cables [25].

is the bipolar. Two 600 MW bipolar circuits will be installed for a total of four cables.

The benefits for the Italian network deriving from this new interconnection, the number twenty-three for the transmission system operator TERNA, are:

- savings for the Italian electricity system up to 150 million euro per year,

- 60% more capacity of interconnection installed, from which follows an increased security of supply,
- increase of the exchange capacity on the French border up to 1200 MW,
- reduction of bottlenecks on the European network,
- creation of more than 500 jobs [25].

2.6 Conclusion

In this chapter a comparison between the HVDC transmission and the AC transmission has been presented, listing the positive aspects of a future multi-terminal HVDC grid. Also a brief description of the CSC and VSC technologies has been given. The advantages of the voltage source converter have been underlined and it can be concluded that the VSC-HVDC system is preferable for the future development of the grid since it facilitates the network extension, the integration of the off shore wind farms and the connection to weak AC systems. Finally, the new interconnection line between Italy and France has been described.

Chapter 3

HVDC System Configurations

3.1 Introduction

This chapter describes the possible configurations for the transmission of power with HVDC systems. A brief insight into the matter of the system grounding is also given.

The existing HVDC lines are mainly end-to-end systems, the only multi-terminal systems (as of 2016) are the SACOI link in Italy, Quebec-New England Transmission system between USA and Canada, the North-East Agra in India (year of commissioning 2016) and the five-terminal system in Zhoushan, China [29][13][30]. The HVDC systems can be built in monopolar or bipolar configuration or a combination of the two. They can also implement different earthing principles: high or low impedance grounding, multiple or single connection to the earth. Currently there is no clarity on the preferred configuration for an MTDC grid and neither for the best grounding. The choice has to be made taking into account some factors such as:

- reliability;
- system costs;
- protection system design;
- extensibility [14].

The term extensibility describes the possibility to tap an additional HVDC link to an already existing grid. In the past with point-to-point lines, it often happened that the investment costs were partially shifted in time, building a monopole initially and then adding a second pole and doubling in this way the transferred power. For a meshed grid it is less straightforward than for a two terminals line, but it is expected that in the process of building an interconnected European HVDC grid, extensibility will be an important aspect.

3.2 Asymmetric monopolar system

This type of configuration consists of a single high voltage cable connecting the converter stations and carrying the full current. The neutral point of the converters is connected to the ground and the current returns through the earth. Alternatively, the return path can consist of a metallic conductor dimensioned for low voltage and grounded at several stations or just at one node of the grid. The first option is called *asymmetric monopole with earth return* and an example can be seen in figure 3.1, the second option is called *asymmetric monopole with metallic return* and it is shown in figure 3.2.

For a cable system, the asymmetric monopole with earth return is the most advantageous configuration in terms of cost. In fact it implements a single conductor to transmit the power and in the project of an HVDC link, cables are the biggest cost [14]. It is however not always simply realizable since in many countries a continuous earth current flow is not acceptable on the basis of environmental concerns. Furthermore, the connection to earth through electrodes has to be designed carefully to avoid corrosion problems.

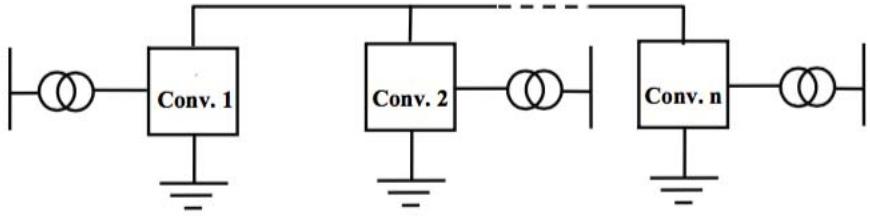

Figure 3.1: Monopole with earth return [14].

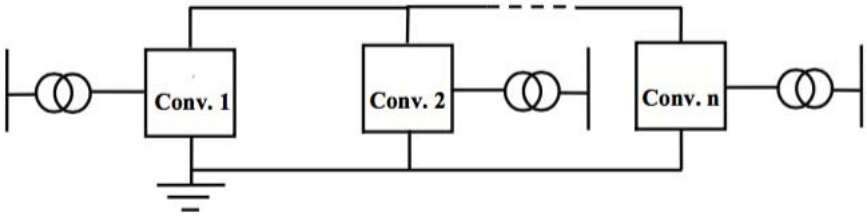

Figure 3.2: Monopole with metallic return [14].

An asymmetric monopolar configuration with metallic return is more expensive since it has an additional cable and the losses, caused by the current flowing through the metallic return, are higher [14]. The insulation for the return conductor is less costly than for the high voltage cable. In fact the cable is normally operated at near zero voltage and it has just to withstand the voltage drop along the conductor during normal operation and the neutral point voltage rise during fault conditions.

3.3 Symmetric monopolar system

In this type of configuration each station consists of a converter connected to the other station by mean of two cables, both at high voltage of the same magnitude but opposite in polarity. As figure 3.3 shows, the ground connection can be done at the middle point of the DC side capacitors or with high value impedance reactors at the AC side [14]. However, if one pole is not available the current cannot flow through the earth return path and the entire active power is lost. The majority of the VSC-HVDC links are realized using a monopolar symmetrical configuration.

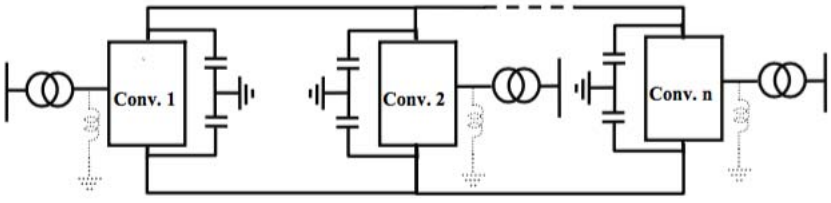

Figure 3.3: Symmetrical monopole [14].

3.4 Bipolar HVDC grid with metallic return

The bipolar configuration is the main interest of this thesis. An example can be seen in figure 3.4. There are two converters per station, the top one is connected to a high voltage-positive polarity conductor and the bottom converter to a high voltage-negative polarity conductor. In-between the two converters of a station there is a connection to the return path. During normal operation the converters in a station are controlled in the same way in order to have zero current flowing in the return path, only in case of active power unbalance between the two poles a current can be registered. If for a monopolar configuration the outage of a converter or of a cable means the outage of the entire link, for a bipolar configuration half of the power can be still exchanged using the return path. This scheme increases hence the overall reliability of the system.

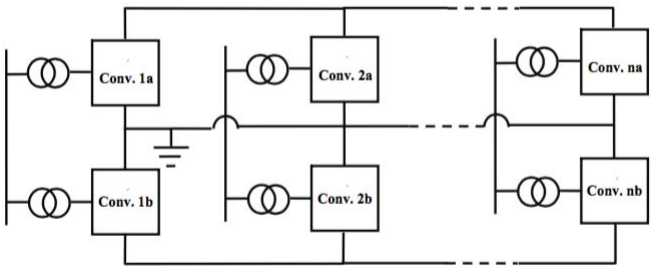

Figure 3.4: Bipolar HVDC grid with metallic return [14].

3.5 Extensibility and grounding of the system

The bipolar configuration with metallic return is well-suited for the development of the future HVDC grid. In fact in terms of extensibility, multiple other links can be connected to a bipole. But first some distinctions have to be made regarding the grounding system. A bipolar link can be low or high impedance grounded. With a low impedance grounding the system is subject to high current but limited voltage during fault conditions. On the contrary, the voltage raises significantly during a fault in a system with a high impedance grounding. When an asymmetric monopole is added to the bipole in a high impedance grounded system, the rating insulation of the asymmetric link neutral conductor has to increase to withstand the voltage stress, resulting more costly. Furthermore in case of an asymmetrical tapping the control is more complex since the system has to work continuously in unbalanced conditions. Other possibilities to extend a bipolar HVDC grid are with symmetric tapping or bipolar links as is shown if figure 3.5.

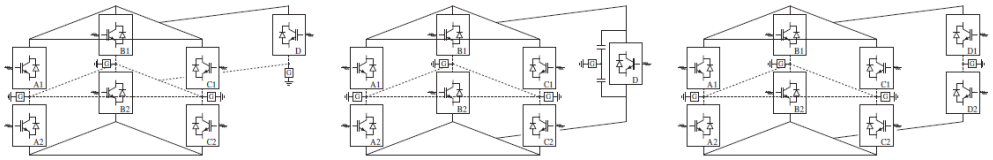

(a) Bipolar grid with metallic return and asymmetric monopolar tappings

(b) Bipolar grid with metallic return and symmetric monopolar tappings

(c) Bipolar grid with metallic return and bipolar tappings with earth return

Figure 3.5: Examples of HVDC bipolar grid development [31]

The high voltage stress during contingencies in a high impedance grounded system is severe and for this reason the low impedance earthing is preferable. The system can be low impedance grounded in one single point of the grid or in several points at the same time. However, if grounding is present in several stations, there is a return path for the current parallel to the metallic return.

Chapter 4

Voltage control in multi-terminal HVDC grids

In a multi-terminal grid it is important to find a quantity to use as a reference value for the control of the converters in the network. Similar to the frequency, which is the control variable for the stability of the AC grid; the DC voltage allows to monitor the power balance between the terminals of a VSC-HVDC grid. In fact, when a node of the grid is subjected to a power step, the whole system experiences a positive variation of current if the power increases at that node, or a negative change if the power decreases. The charge of the capacities (converters and lines cable capacitances) follows a positive variation of current in the system and the discharge of the capacities corresponds to a negative variation. In the first case the voltage at every node of the grid increases and in the second case it decreases. The capacities in the system react to the change of power injected or withdrawn storing energy like in the AC system is done by the rotating masses, with the difference that the inertia of the rotating masses is much bigger. The time constant in the DC grid is in the order of milliseconds for the primary control and in the order of seconds for the secondary control [32]. Differently to the frequency in the AC grid, the voltage has not the same value at each node of the DC grid. In fact the impedance of the line has to be taken into account, thus the voltage drop. The actual value of the voltage at every terminal can be found only after a power flow calculation.

4.1 Centralized voltage control

The control strategy adopted for a two-terminal HVDC link consists in a terminal fixing the active power and the other the DC voltage. In this way the active power is balanced if the voltage is kept constant. Figure 4.1 shows the control characteristics applied to the two converters, figure 4.1(a) refers to the constant power mode, 4.1(b) to the constant voltage.

In a multi-terminal grid, the aforementioned logic can still be applied. One converter in the grid sets the voltage level at its bus, behaving as a slack bus, all the other converters apply a constant active power control. In this operating mode, when a contingency occurs in the grid, the voltage controlling converter is the only one changing its power output in order to maintain the voltage value constant. For a correct stable operation it is important that not more than one converter controls the voltage.

Despite the simplicity of this control strategy, defined also as *centralized control*, it is not probable that in a future meshed grid one single slack bus will be used to maintain the voltage between the tolerance boundaries. The centralized strategy lacks one of the most important properties required in a control system, i.e. reliability. In fact the larger the grid, the larger the disturbances that the slack bus has to damp. The capability of the voltage controlling converter can be insufficient to handle these perturbations. Furthermore big and sudden changes in the power output of a converter have a severe impact on the AC side near to the converter. If then the grid is interconnected between different countries, it would be difficult to find a TSO that would take the burden of having such a slack "bus" in his country.

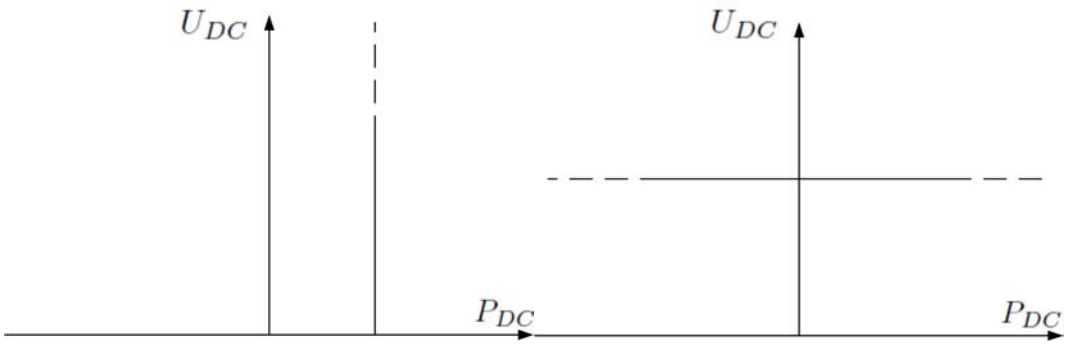

(a) Fixed power characteristic (b) Fixed voltage characteristic

Figure 4.1: Centralized control characteristics

A possible solution is to provide a backup control, that is a converter switching from power to voltage control when the slack bus is incapable to face the disturbance. Such a backup control is however more suited for small grids. In grids where perturbations are large, changes in operational mode will occur more often leading to a highly non-linear system behavior that causes the loss of dependency between the local voltage measurements and the general state of the system [21].

4.2 Distributed droop control

To face the discussed problems, another control strategy has been studied for large HVDC grids, the *distributed control*. It is an operation mode already used in AC grids and implements a proportional action. In this way, every converter modifies its power output proportionally to the voltage variation at its grid node after an outage or a disturbance. The use of a proportional controller leads to a steady-state voltage deviation after the primary control action. The characteristic of the droop can be seen in figure 4.2 where voltage is displayed as a function of the current (it is also possible to express the voltage as a function of power).

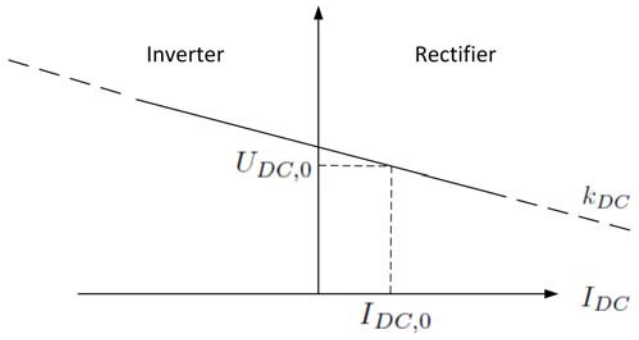

Figure 4.2: DC voltage droop characteristic

As an input for the controller, a set-point ($U_{DC,0}$, $I_{DC,0}$) is needed. It can be obtained from a power flow calculation. For more detail the reader is referred to Appendix A. The other important parameter is the droop constant k_{DC} which coresponds to the slope of the characteristic and is also the inverse of the proportional controller gain g_{DC}. In this thesis, current and power are positive when entering the DC system, thus they are positive for a converter in rectifier mode and negative in inverter mode. As a consequence, the slope of the droop characteristic is negative. The relation between current and voltage can be written as

$$\Delta I_{DC} = -\frac{1}{k_{DC}} \Delta U_{DC} \tag{4.1}$$

where $\Delta I_{DC} = I_{DC} - I_{DC,0}$ and $\Delta U_{DC} = U_{DC} - U_{DC,0}$ are the current and voltage variations with respect to the initial set-point. As an alternative, the droop characteristic can be written in terms of power and voltage, as it is done in [33][34]. Hence, the droop law is written as

$$\Delta P_{DC} = -\frac{1}{k_{DC}} \Delta U_{DC} \tag{4.2}$$

where $\Delta P_{DC} = P_{DC} - P_{DC,0}$ is the difference between the actual power output of the converter and the reference set-point. The V-I characteristic is more connected to the dynamics of the system and is a more realistic control since it proportionally relates two linearly dependent variables [35]. The P-V characteristic behaves identically around the set-point, but for larger deviations, the difference between the two representations increases as well due to the quadratic relation between the variables. The advantage of the power-voltage droop is the easier integration in the outer loops and the easier computation of power flows.

The value of the droop constant is an indication of how much a converter will change its power output to stabilize the voltage. The lower the droop constant, the more the converter adapts its output power at voltage variations; the limit with $k_{DC} = 0$ gives us the constant voltage control characteristic. On the contrary, a high value of the droop constant causes the converter to tolerate a high steady-state error at the DC voltage while having a low variation in the power output; in this case the limit for k_{DC} tending to infinity gives a constant current/power characteristic.

The droop controller has the local voltage measurement as input. In this way there is no need for communication between the different nodes of the grid and a fast response to the variation is assured. Anyway, it has also been proposed to use a common voltage feedback [26,33], with the result of independence between the change of power sharing and the nodal voltage variation. The droop control law in this case becomes:

$$I_{DC} = I_{DC,0} - \frac{1}{k_{DC}} (U_{DC}^{comm} - U_{DC,0}^{comm}) \tag{4.3}$$

with U_{DC}^{comm} the common feedback signal and $U_{DC,0}^{comm}$ its reference. The disadvantage of this approach is the need of communication.

In the meshed multi-terminal system the use of a distributed control is more advantageous for the following reasons:

- every converter changes its output in accordance with its droop characteristic. As a result, every terminal takes a share in the compensation of the disturbances;
- the action does not rely on communications between different terminals but only on local voltage measurements. Therefore, it guarantees also a fast response;
- the control is very simple since it is proportional;
- it is a reliable strategy and it has a N-1 security criterion [35].

4.3 Control strategies simulation

In this section of the thesis different control strategies have been applied to show their working principle in a three-terminal monopolar VSC-HVDC grid (shown in figure 4.3), consisting of one rectifier and two inverters. This system can for example represent a wind farm connected to two load systems. The description of the design of the control and of the grid model is postponed to the next chapter.

4.3.1 Centralized control

In this simulation, the rectifier operates in a power control mode, inverter 1 controls the voltage and inverter 2 operates in power control. The AC grid voltage is 380 kV while the power rating of the converters is 1200 MVA. After one second, a power step of $\Delta P_{DC,rec} = -120$ MVA is

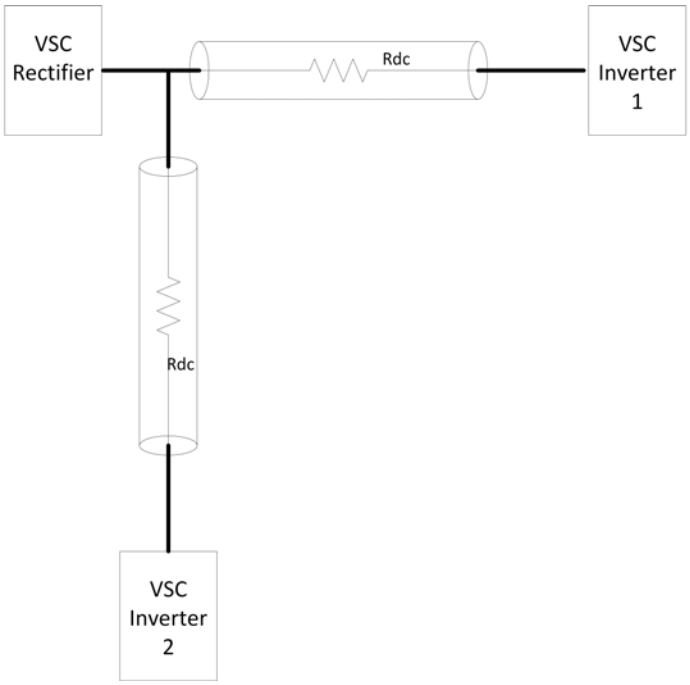

Figure 4.3: Three terminals monopolar VSC HVDC grid

Table 4.1: Simulation results of a centralized control strategy

Initial Values:	**Power [pu]**	**Voltage [pu]**
Rectifier	0.5	1.009
Inverter 1	-0.295	1
Inverter 2	-0.2	0.9965
After the contingency:	**Power [pu]**	**Voltage [pu]**
Rectifier	0.4	1.007
Inverter 1	-0.1975	1
Inverter 2	-0.2	0.9965

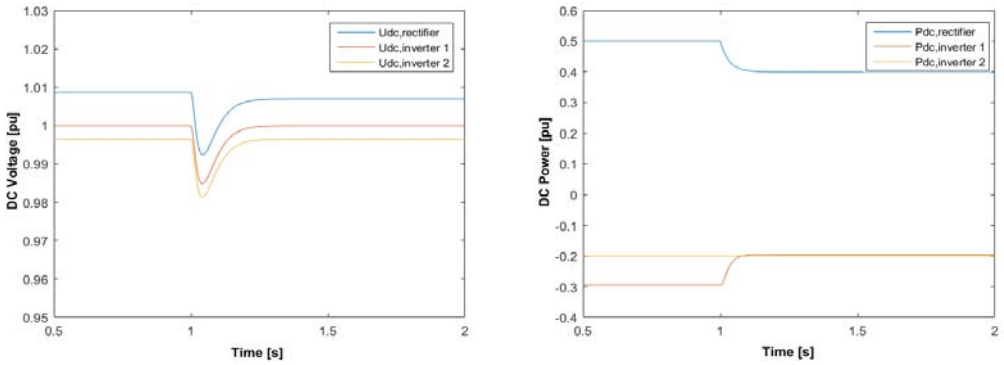

(a) Grid nodes voltage profile

(b) Converters power output

Figure 4.4: Centralized control characteristics

applied to the rectifier to simulate a drop in generation. Table 4.1 lists the set-points of the converters before and after the power step. In figure 4.4 (a) the grid nodes voltages are plotted as function of time, while in figure 4.4 (b) the power output of the three converters can be found.

The power balance is reestablished after the contingency thanks to the action of inverter 1. It changes substantially its power output to keep the voltage constant. On the contrary, the power output of inverter 2 remains the same.

A second simulation shows the case of possible failure of the centralized control when a big power imbalance occurs. The grid and voltage rating are the same as in the previous case and the working set-points before and after the power step applied at the rectifier control input can be found in table 4.2. Also in this case a power step is applied at the rectifier control input, this time the lack of generation is much bigger, half of the rated power, $\Delta P_{DC,rec} = -600$ MVA. It can be seen in figure 4.5 that the only way inverter 1 is able to keep the voltage constant

Table 4.2: Simulation results of a centralized control strategy

Initial Values:	**Power [pu]**	**Voltage [pu]**
Rectifier	1	1.0172
Inverter 1	-0.274	1
Inverter 2	-0.7	0.9876
After the contingency:	**Power [pu]**	**Voltage [pu]**
Rectifier	0.5	1.009
Inverter 1	0.213	1
Inverter 2	-0.7	0.9876

is to switch from inverter operation to rectifier mode. This is not possible if the inverter is connected to a system were no generation is available. Hence, the node that implements the voltage control has to be chosen carefully, since it has the burden of compensating the whole power unbalance and of tolerating an important stress at the AC side caused by the sudden change of power reference. The consequences of a missed control action are a even bigger voltage variation.

4.3.2 Distributed control

The same grid as the previous examples is now operated in a distributed control mode. In particular, the rectifier is controlling the power. At its control input a power step of -0.5 [pu] is given at the moment in time of 1 second, while the two inverters are both implementing a droop control. Accepting a voltage steady state variation of 7% the value chosen for the droop

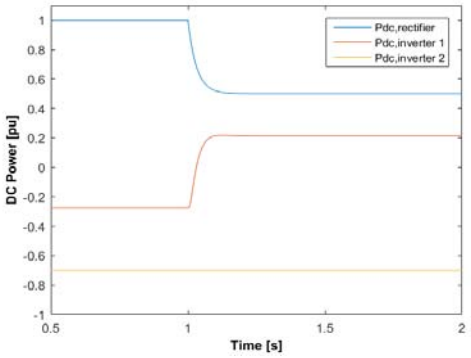

Figure 4.5: Converters power output simulation number 2

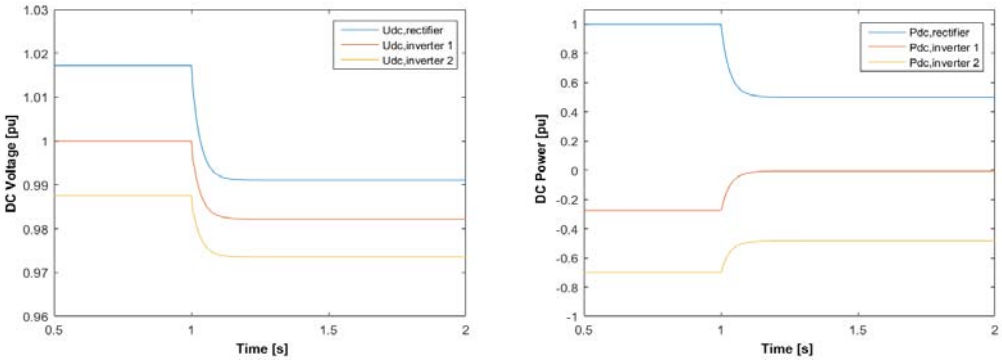

(a) Grid nodes voltage profile

(b) Converters power output

Figure 4.6: Decentralized control characteristics

constant is $k_{DC} = 15$, equal for both inverters. The voltage and power values resulting from the simulation are listed in table 4.3 and the voltage and power profiles are shown respectively in figure 4.6 (a) and 4.6 (b).

Table 4.3: Simulation results of a distributed droop control strategy

Initial Values:	**Power [pu]**	**Voltage [pu]**
Rectifier	1	1.0172
Inverter 1	-0.274	1
Inverter 2	-0.7	0.9876
After the contingency:	**Power [pu]**	**Voltage [pu]**
Rectifier	0.5	1.009
Inverter 1	0.213	1
Inverter 2	-0.7	0.9876

It is evident how the power imbalance is shared between the two inverters as they both vary their power output proportionally to the voltage variation. The result is a new steady state operating point for the grid. The value of $k_{DC} = 15$ has to be chosen as a function of the acceptable steady state voltage variation at the grid nodes. Furthermore, it influences the size of the share that a converter will take in compensating the power imbalance. The lower the droop constant in a converter controller, the larger the unbalanced power share for that converter.

4.4 Conclusion

The centralized and distributed voltage control strategies have been described. The centralized control implements a constant voltage compensator at one converter and a constant power controller at the other terminals. After a disturbance, the only converter controlling the voltage has the burden of compensating the unbalanced power.

The distributed control implements the droop compensator at each node of the DC grid. It reacts to a voltage variation and balances the power in the network by changing the current output of the VSC. In this way all the converters contribute to the primary control.

Finally two simulations show the working principle of the control strategies in a three terminals monopolar VSC-HVDC grid. The distributed control resulted the most reliable method for the voltage control in the multi-terminal network.

Chapter 5

Modelling and control of a bipolar MTDC grid

5.1 Introduction

This chapter describes how to model a VSC converter and a bipolar MTDC grid. Different control design techniques of the VSC are also studied and implemented in the model. The validation is done by mean of simulations using MATLAB Simulink. The model is then used to analyze the dynamic stability of the system after a contingency, focusing on the bipolar grid configuration.

5.2 Averaged model

To study the dynamic behavior of the system, an averaged converter model is used. It is a reduced order model, since it disregards the switching process of the converter. Thus the resulting model is generic, it does not depend on the converter technology or on the modulation technique used to synthesize the converter voltage waveform. As explained in [36], the correct way to derive a simplified model is to eliminate the very small time constants of the system, such as the time constant of the switching process of the power electronics or that of the DC line current dynamics. The advantages of doing this are the reduction of the number of differential equation governing the system and the acceleration of the calculations, as it is possible to increase the integration step size in the simulations. The averaged model is used to study the stability of the system through the dynamics of the average values of the variables. In the following sections all the components of the VSC-HVDC system are modeled.

5.2.1 Voltage Source Converter

Although the converter is characterized by discrete switching states, for control purpose the VSC can be modeled in a simplified way by decoupling the AC side from the DC side [37]. At the AC side, the converter is modeled as a voltage source whereas at the DC side it is modeled as a current source connected to a capacitor. Figure 5.1 represents the averaged model of the VSC converter.

If internal losses of the converter are neglected, AC and DC sides are linked by the power balance in the converter. The current through the DC generator can thus be written as

$$I_{DC} = \frac{P_s}{U_{DC}} \tag{5.1}$$

where U_{DC} is the voltage at the DC side capacitor and P_s is the active power flowing from the AC side to the converter.

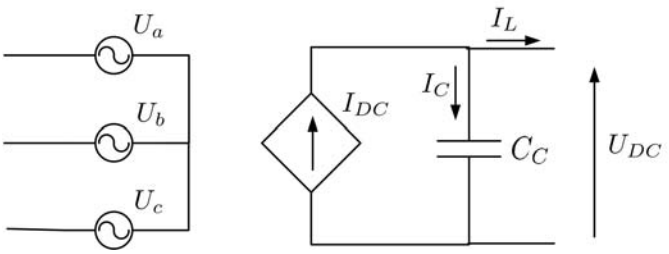

Figure 5.1: VSC averaged model

The fundamental equation of the capacitance allows us to calculate the direct voltage U_{DC} since

$$I_{DC} - I_L = I_C = C_C \frac{dU_{DC}}{dt} \tag{5.2}$$

where I_L and I_C are respectively the DC line current and the current through the capacitor C_C that represents the internal capacitance of the converter. C_C is responsible of the reduction of the generated voltage ripple [38]. Thus the stabilized voltage has a well-defined level and it can be considered independent from the switching process of the VSC. The converter capacitance is also designed to achieve an optimal dynamic behavior after a change of the converted power. In fact, it affects the power exchanged between AC and DC side since it acts as a energy buffer [39]. A small value of the capacitance means that the reaction to a change is fast. Usually the capacitance size is expressed in terms of the time constant τ_C.

5.2.2 Line or Cable Model

As explained before in chapter 3, a bipolar HVDC configuration is made of two cables and possibly a metallic return conductor operating at near zero voltage. During normal operation the two cables are at opposite voltage, equal in magnitude, and the metallic return conductor does not carry any current. From a dynamic point of view a model that represents the cable transients is shown in figure 5.2. It is a π model of the DC transmission line and it includes the series of an inductance, a resistance and two capacitances. The values of these parameters are:

$$R_{DC} = r_{DC} x \tag{5.3}$$

$$C_{DC} = c_{DC} x \tag{5.4}$$

$$L_{DC} = l_{DC} x \tag{5.5}$$

with x the length of the cable, r_{DC}, c_{DC} and l_{DC} respectively the resistance per length, capacitance per length and inductance per length. For a more simplified analysis the cable inductance L_{DC} can be initially neglected, hence disregarding the DC current dynamics. This translates in the elimination of currents as state variables [21].

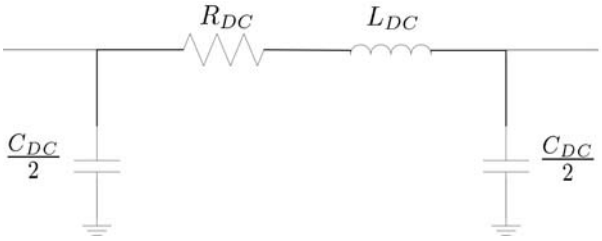

Figure 5.2: pi-model of a DC transmission line

5.2.3 AC reactor

The AC side of the converter is modeled as a controlled voltage source, while an alternating voltage generator represents the AC grid. A complex impedance $\underline{Z_s} = R_s + jX_s$ connects the converter with the point of common coupling and includes the converter reactor, responsible for smoothing the current harmonics, and the transformer inductance [40]. In figure 5.3 the impedance is shown.

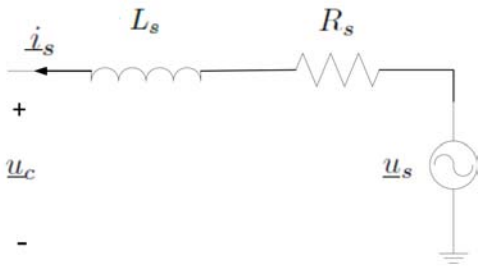

Figure 5.3: Converter AC voltage and grid voltage

5.3 Control design

To maintain the stability, the control system of a VSC has to regulate the value of real and reactive power exchanged between the VSC system and the AC grid at the Point of Common Coupling (PCC). There are two control modes that can be used: *voltage-mode control* and *current-mode control*. Implementing the first mode, the power components (real power P_s and reactive power Q_s) are controlled by the phase angle and the magnitude of the VSC voltage at the AC side with respect to the voltage at the PCC [40][41][42]. Neglecting the line resistance, the equations that describe this control mode are

$$P_s = \frac{U_c U_s \sin\delta}{X_s} \tag{5.6}$$

$$Q_s = U_s \frac{U_c \cos\delta - U_s}{X_s} \tag{5.7}$$

where U_c is the converter AC side voltage, U_s is the AC grid voltage, δ is the angle between the two voltages and X_s is the reactance of the inductor L_s in figure 5.4.

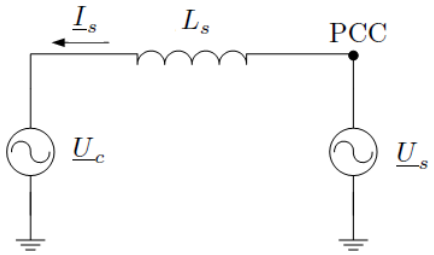

Figure 5.4: VSC AC side and AC system representation

If U_c and U_s are close enough in terms of angle and magnitude, the real and reactive power controls are almost decoupled and they can be operated independently. The active power becomes a function of the angle

$$P_s = f(\delta), \tag{5.8}$$

and the reactive power a function of the VSC voltage magnitude

$$Q_s = f(U_c). \tag{5.9}$$

Figure 5.5 shows the sign of the active and reactive power through vector diagrams. In particular, if U_c phase lags U_s the direction of the active power is positive and the VSC works in rectifier mode, figure 5.5 (a); if U_c phase leads U_s, the real power is negative and the VSC operates as an inverter, figure 5.5 (b).

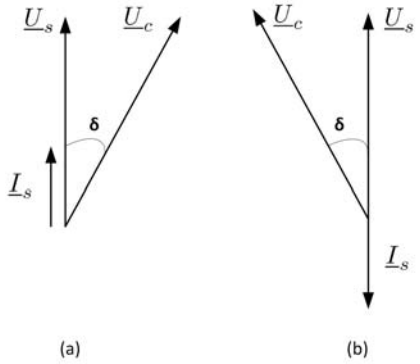

Figure 5.5: Active power flow vector diagram

The sign of the reactive power is then dependent on the different amplitude of the voltages U_c and U_s as depicted in figure 5.6 where the phase angle δ has been set to zero. In particular if $U_s > U_c cos\delta$ there is reactive power consumed from the ac network, figure 5.6 (a); if $U_s < U_c cos\delta$ there is reactive power generated into the AC network, figure 5.6 (b).

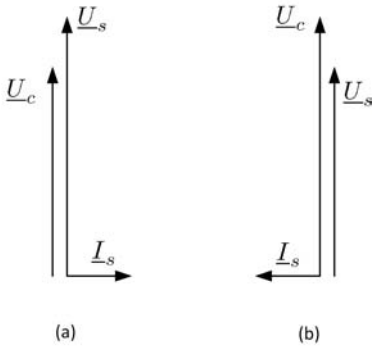

Figure 5.6: Reactive power flow vector diagram

The *voltage-mode control* is not further described as in this thesis a *current-mode control* has been implemented in the model used for the simulations. Voltage-mode control has not been chosen because it does not allow the protection of the VSC against overcurrents that can appear when the commands are rapidly changed or when a fault occurs in the AC side [40]. When instead a current-mode control is used, limits can be imposed to line currents protecting the converter against overload conditions. Other advantages are a superior dynamic performance, a higher control precision and a more robust response to oscillations of VSC and AC system parameters [43]. Equations (5.6) and (5.7) can be modified to show the relation with the line current I_s

$$P_s = U_s I_s \cos\varphi \tag{5.10}$$

$$Q_s = U_s I_s \sin\varphi \tag{5.11}$$

where φ is the angle between the vector of the line current and the vector of the AC voltage at the PCC as it is shown in the vector diagram of figure 5.7.

Hence in the current control approach, the VSC line current is firstly adjusted by a dedicated control loop, through the VSC AC side voltage. Then, both active and reactive power are

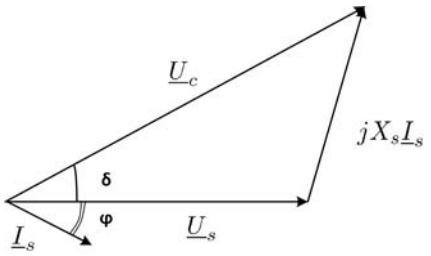

Figure 5.7: Vector Diagram of VSC AC side voltage and current

controlled acting on phase angle and amplitude of line current with respect to AC system voltage at PCC [40].

A reference frame transformation is normally applied to the control variables to allow the analysis of the power exchange in a vector mode. The Park's transformation is implemented in order to obtain DC signals waveforms in steady-state condition [44]. As a result, the control system has a simpler design and the equations that govern it have a lower dynamic order. The rotational speed of the *dq*-frame is chosen equal to the speed of the AC currents and voltages phasors and the frame is synchronized with the system voltage. Considering positive the power and the current entering the DC system as depicted in figure 5.4, the relations connecting real and reactive power with line current and AC voltage in the *dq* frame are

$$p_s = \frac{3}{2}[u_{sd}i_{sd} + u_{sq}i_{sq}] \tag{5.12}$$

$$q_s = \frac{3}{2}[u_{sq}i_{sd} - u_{sd}i_{sq}] \tag{5.13}$$

where u_{sd}, u_{sq} and i_{sd}, i_{sq} are respectively the d and q components of AC voltage and current phasors. These equations can be further simplified if the transformation rotating frame is synchronized with the AC voltage resulting in $u_{sq} = 0$ and thus equations (5.12)-(5.13) become

$$p_s = \frac{3}{2}u_{sd}i_{sd} \tag{5.14}$$

$$q_s = -\frac{3}{2}u_{sd}i_{sq} \tag{5.15}$$

demonstrating that the two current components can control the real and reactive power exchange at the PCC separately. In the practical control implementation this action of synchronization is done by the Phase Locked Loop (PLL) [45][46][47]. The PLL action has to ensure that the space phasor of the AC grid voltage $\underline{U}_s(t)$ is aligned with the d-axis of the *dq*-frame. The phase locked loop is a control system that receives as input the AC voltage phasor and generates as output the required angle for the Park's transformation. With the cascaded actions of a phase detector, a loop filter and a voltage controlled oscillator (in the basic configuration), the PLL generated angle ρ is such as

$$\rho(t) = \omega_0 t + \theta_0 \tag{5.16}$$

with ω_0 the pulse of the AC voltage and θ_0 its initial phase angle.

The control scheme for VSC is made of two levels: an outer loop that receives as inputs the references for the controlled variables (P_s, Q_s, U_{DC}, U_{AC}) producing as outputs the reference values of the current components (i_{sdref}, i_{sqref}) and an inner loop that tracks the current references arriving from the outer loop. It is important for the stability of the control system that the inner loop has a much faster response compared to the outer loop.

5.3.1 Current or internal controller

At the nodes of the grid where current control is applied, the converter internal controller has to deal with the tracking of current references. The response of the system to the control action

depends on how the converter is modelled and is governed by a first order equation describing the series of a resistance R_s and an inductance L_s, as depicted in figure 5.3.

Thus, the equations of the converter AC side dynamics are firstly studied and then related to the control system. With respect to figure 5.3, the dynamics of the AC side are expressed by

$$L_s \frac{di_s}{dt} + Ri_s = u_s - u_c \tag{5.17}$$

Applying the Park's transformation and synchronizing the rotating frame d-axis with the space phasor of the AC grid voltage ($u_{sq} = 0$), equation (5.17) becomes

$$L_s \frac{di_{sd}}{dt} + Ri_{sd} = L_s \omega i_{sq} + u_{sd} - u_{cd} \tag{5.18}$$

$$L_s \frac{di_{sq}}{dt} + Ri_{sq} = -L_s \omega i_{sd} - u_{cq} \tag{5.19}$$

where i_{sd} and i_{sq} are state variables, u_{cd} and u_{cq} are control inputs and u_{sd} is a disturbance input. The plant model block diagram is shown in figure 5.8. It results from equations (5.18) and (5.19) after applying the Laplace transformation.

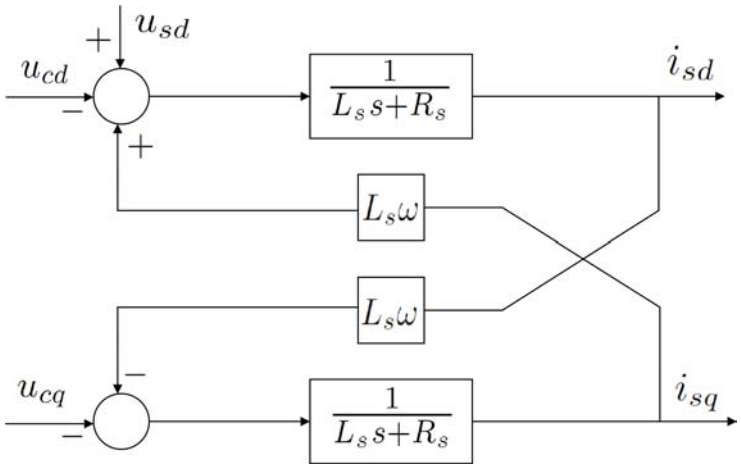

Figure 5.8: Converter block diagram, control system plant

The plant equations are dynamically coupled due to the terms $L_s \omega i_{sq}$ and $-L_s \omega i_{sd}$. A decoupling is therefore implemented in the inner loop

$$u_{cd} = -u_d + L_s \omega i_{sq} + u_{sd} \tag{5.20}$$

$$u_{cq} = -u_q - L_s \omega i_{sd}. \tag{5.21}$$

where u_d and u_q are the new control inputs [48][49]. Substituting equations (5.20) (5.21) in (5.18) and (5.19), two decoupled first-order linear systems are obtained

$$L_s \frac{di_{sd}}{dt} + Ri_{sd} = u_d \tag{5.22}$$

$$L_s \frac{di_{sq}}{dt} + Ri_{sq} = u_q. \tag{5.23}$$

The inputs are provided by a compensator that elaborates current errors, i.e. the difference between a reference value and the dq components of the measured line current ($e_d = i_{sdref} - i_{sd}$ and $e_q = i_{sqref} - i_{sq}$), with the purpose of reducing it to zero. This control action is undertaken by a Proportional Integral (PI) controller [50].

Figure 5.9 shows the inner control loop in a block diagram. To obtain it, the Laplace transformation is applied to the previous equations.

Figure 5.10 shows a simplified diagram d-axis and q-axis of the closed loop controllers that includes also an Anti-Wind-Up (AWU), necessary to avoid the integral error when the variables hit their limits.

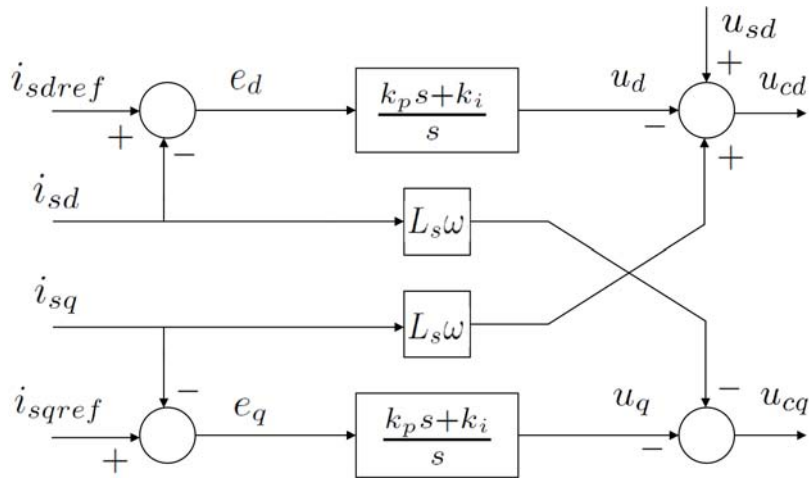

Figure 5.9: Decoupled inner current controllers

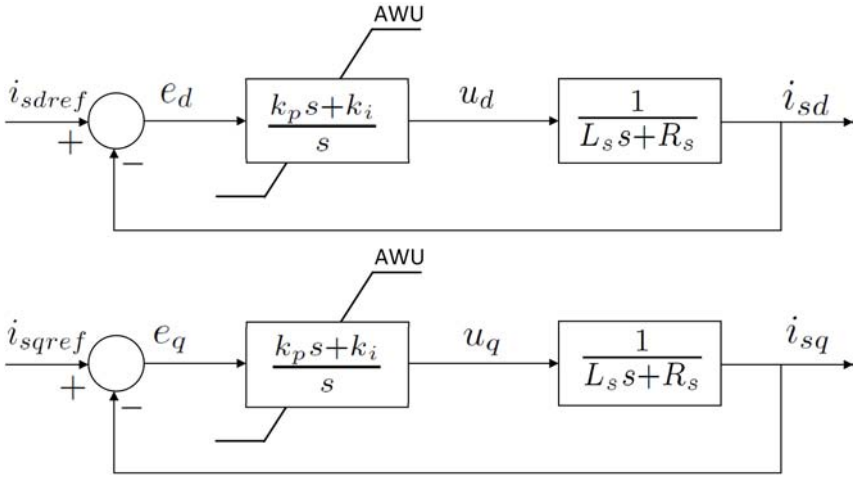

Figure 5.10: Simplified block diagram of the current controller

The transfer function of the PI compensator has been written in the diagram as

$$G_{PI}(s) = \frac{k_p}{s} + k_i s \tag{5.24}$$

where k_p and k_i are respectively the proportional gain and the integral gain. These two constants have to be tuned in order to achieve fast response and stability, the *"modulus optimum"* technique is used for this purposes [51]. With this strategy, simplification of the dynamic equations is achieved through pole cancellation. The resulting values of the PI controller gains are

$$k_p = \frac{L_s}{\tau_i} \tag{5.25}$$

$$k_i = \frac{R_s}{\tau_i}. \tag{5.26}$$

with τ_i the time constant of the closed loop. τ_i is a design choice and it should be small enough to guarantee a fast response, but not too small such that $\frac{1}{\tau_i}$, that is the closed control loop bandwidth, is smaller than the limit dictated by the switching frequency of the VSC. Typically $\tau_i = 0.5 - 5$ ms [40], in [52] a bandwidth of 320 Hz has been used to guarantee a dynamic response with no overshoot.

The remainder of the thesis will focus on the regulation of the active power, disregarding the analysis of the reactive power control system.

5.3.2 Outer controllers

The outer controllers are directly connected with the inner control loop and they produce the reference current. The controllers described in this section are the constant active power regulator, the constant DC voltage regulator and the DC voltage droop controller.

Constant power controller

The active power control closed loop of figure 5.11 includes a PI compensator that is responsible of tracking perfectly the power reference received as input. The plant and the current control loop have been represented as a first order system with time constant τ_i, as this is the result of the proper tuning of the current controller. Also the power compensator is tuned with a *"modulus optimum"* strategy with a bandwidth that has to be one order of magnitude smaller ($\approx$ 30 Hz) to ensure that the outer loop is slower than the inner loop [52]. The proportional and integral gains of the transfer function of the power PI controller are

$$k_{pp} = \frac{\tau_i}{\tau_p u_{sd}} \tag{5.27}$$

$$k_{ip} = \frac{1}{\tau_p u_{sd}} \tag{5.28}$$

where τ_p is the time constant of the closed loop.

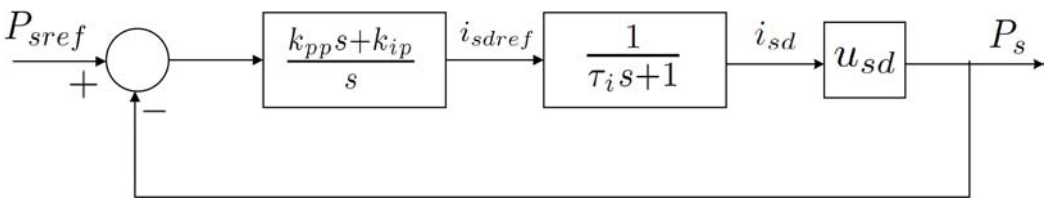

Figure 5.11: Block diagram of the constant active power controller

Constant DC voltage controller

The design of the outer control loop for the DC voltage depends on the strategy chosen for the control action. The first design described is similar to the power outer loop, in fact also in this case it consists of a PI compensator that receives the difference between a DC voltage reference and a DC voltage measure as input and aims at setting this error to zero. The block diagram of figure 5.12 represents the closed loop. In this case, a stable response is obtained by tuning the PI compensator with the *"symmetrical optimum"* criteria [51]. The block diagram of figure 5.12 represents the DC link dynamics, expressed by the differential equation

$$i_{DC} - i_L = C\frac{du_{DC}}{dt} \tag{5.29}$$

where i_{DC} is the converter current, i_L is the current of the DC line and u_{DC} is the DC side voltage, that is measured between the terminals of the DC side capacitor in the averaged model of figure 5.1.

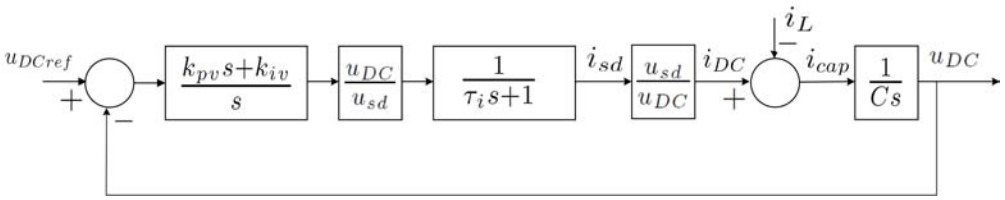

Figure 5.12: Block diagram of the constant DC voltage controller

The interaction between the AC side and the DC side is finally given by the equality of the power at DC side with the real power at AC side

$$u_{DC}i_{DC} = \frac{3}{2}u_{sd}i_{sd}. \tag{5.30}$$

Equation (5.30) holds when converter and commutation losses are neglected.

DC voltage droop controller

The droop control strategy, the main focus of this thesis, has a different control design than the previous. The droop controller is a proportional compensator with a gain that is the inverse of the droop constant k_{DC}. As shown in figure 5.13, the droop controller makes the current reference for the inner loop react to a variation of voltage measured at the DC bus. The variation is detected as the difference between the measured value and the set point. Contrary to the other outer loops described above, the droop controller does not track a reference value, in fact the consequence of the droop action is a steady state voltage error. The magnitude of the error depends on the droop constant. The purpose of this control strategy is to balance the power in the DC grid by changing the current injected by the converter and allowing only a limited variation of the DC voltage.

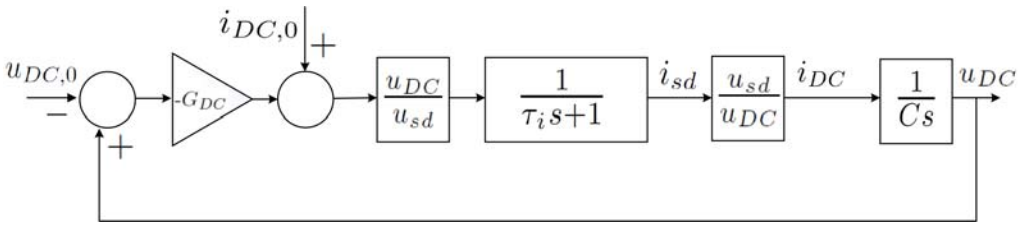

Figure 5.13: DC voltage droop controller

There are multiple ways to design the value of the constant $G_{DC} = \frac{1}{k_{DC}}$. The choice of the gain can be done in order to optimize a variable or to find a trade-off between conflicting aspects,

such as converter ratings or AC and DC systems dynamic stability. A more detailed explanation will be given in chapter 6. In the following simulations the tuning of the proportional droop gain is done in order to optimize the dynamic response of the controller. The regulator has to approximately act on a second order system and the transfer function of the closed loop is

$$G_{CL}(s) = \frac{1}{s^2 \frac{\tau_i C}{G_{DC}} + s \frac{C}{G_{DC}} + 1}, \tag{5.31}$$

that characterize a signal with damping ratio ξ and a natural frequency ω_n

$$\xi = \frac{1}{2\tau_i \omega_n} \tag{5.32}$$

$$\omega_n = \sqrt{\frac{G_{DC}}{C\tau_i}} \tag{5.33}$$

Selecting a damping ratio of $\xi = 0.7$, it is possible to obtain a good dynamic performance and thus to calculate the gain of the proportional compensator.

5.4 Simulation of a converter outage, dynamic results

The model and control design described in the previous section can be used to simulate a monopolar or bipolar grid configuration with the only difference between the two configurations that in a bipolar grid configuration there are two converters and two separate control systems at every node.

The aim of these simulations is to understand how the unbalanced operation that follows a VSC outage can affect the DC voltage control in a bipolar configuration. When a droop control is implemented, a local DC voltage measurement forms the input of the compensator that maintains the power balance. In a bipolar multi-terminal HVDC grid, the DC voltage is measured at every terminal between the pole and the neutral conductor, therefore its value can be affected by the shifting of the voltage at the ground nodes. A dynamic balance of the two poles might be required to achieve a new stable operating point.

5.4.1 Bipolar end-to-end line

In the fist simulation, droop control is used in the VSC of a simple end-to-end bipolar line that can be for example the connection of an offshore wind farm with the mainland. At one side there are two VSCs operating in rectifier mode, at the other side two VSCs in inverter mode. Figure 5.14 represents the link and table 5.1 lists the grid and control parameters.

Table 5.1: Grid and control parameters

Grid Parameters		**Droop Parameters**	
Rated Power	1200 [MW]	Gdc (droop gain)	2.8810
Rated Voltage	380 [kV]	Vdc,0 Rect	1 [pu]
Rdc	0.0175 [pu]	Idc,0 Rect	0.545 [pu]
Rdcm	0.0175 [pu]	Vdc,0 Inv	0.9912 [pu]
line length	150 [km]	Idc,0 Inv	-0.545 [pu]

Initially, the opposite poles are working with identical power output and voltage values, which is called balanced operation. After 1 second an outage of the rectifier in the positive pole takes place. The power goes immediately from 600 MW to zero. Table 5.2 shows the results of the simulation, which are also visualized in figures 5.15 (a) and (b). It is clear that also the power output of the inverter in the positive pole goes to zero after the outage taking all the power share necessary to balance the grid. This happens because the two poles tend to behave like separate systems. The variation of the power and voltage that is registered in the negative

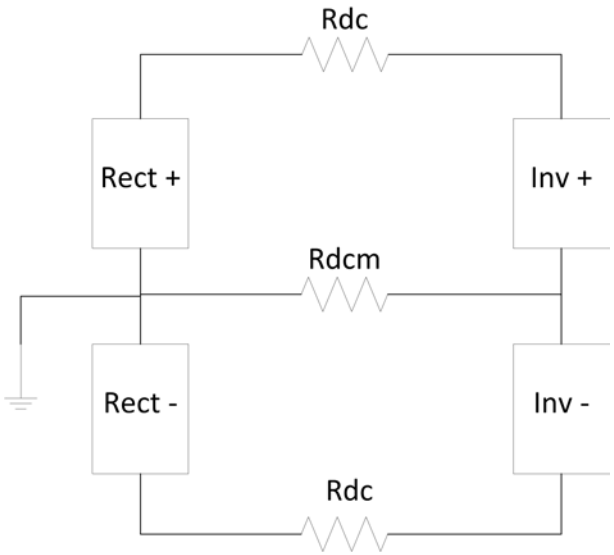

Figure 5.14: Bipolar end-to-end representation

Table 5.2: Simulation results of the outage of the rectifier in the positive pole

Initial Values:	**Power [pu]**	**Voltage [pu]**
Rectifier +	0.5045	1
Rectifier -	0.5045	1
Inverter +	-0.5	0.9912
Inverter -	-0.5	0.9912
After the contingency:	**Power [pu]**	**Voltage [pu]**
Rectifier +	0	0.808
Rectifier -	0.494	1.004
Inverter +	0	0.817
Inverter -	-0.486	0.987

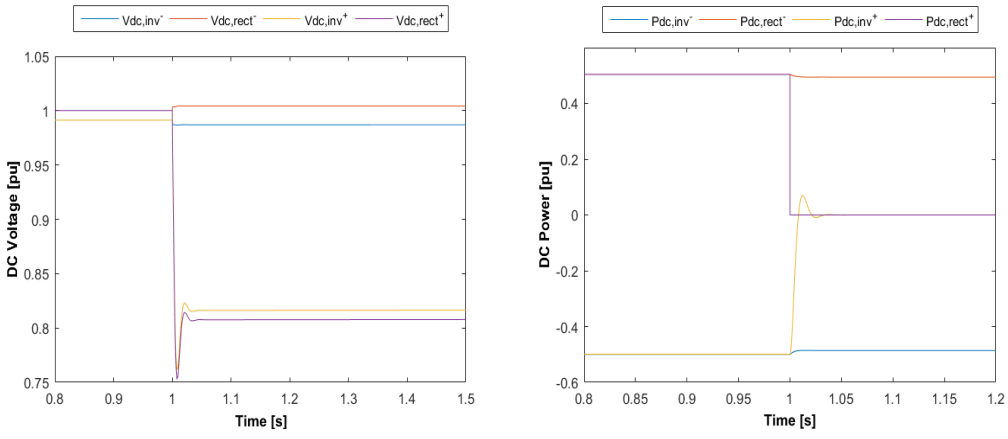

(a) DC voltage profile

(b) Power profile

Figure 5.15: Simulation results of a rectifier outage in a bipolar two terminals VSC-HVDCgrid

pole is much smaller and occurs because of the unbalanced current that starts to flow on the metallic return and that causes the voltage at the neutral nodes to shift.

As proposed in [53], a more realistic model of cable could also be used or the interactions with the AC side could be included [54][55][56]. As an example, figures 5.17 (a) and (b) show the result of the simulation number one when a cable π model made of the three parallel branches is implemented (as done in [53]). The values of the resistances and the inductances of the cable model are listed in table 5.3 and the model is shown in figure 5.16. Stability is reached also in this case, the difference is in the dynamic response of the negative pole.

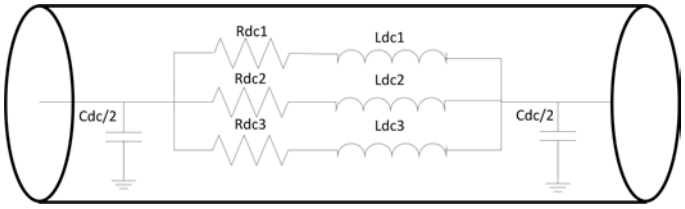

Figure 5.16: DC Cable Model

Table 5.3: Grid and control parameters

Cable Model Parameters	[pu]		[pu]
$R_{dc,1}$	6.6186	$L_{dc,1}$	0.4712
$R_{dc,2}$	0.3036	$L_{dc,2}$	0.2366
$R_{dc,3}$	0.0399	$L_{dc,3}$	2.1913
C_{dc}	1.8325		

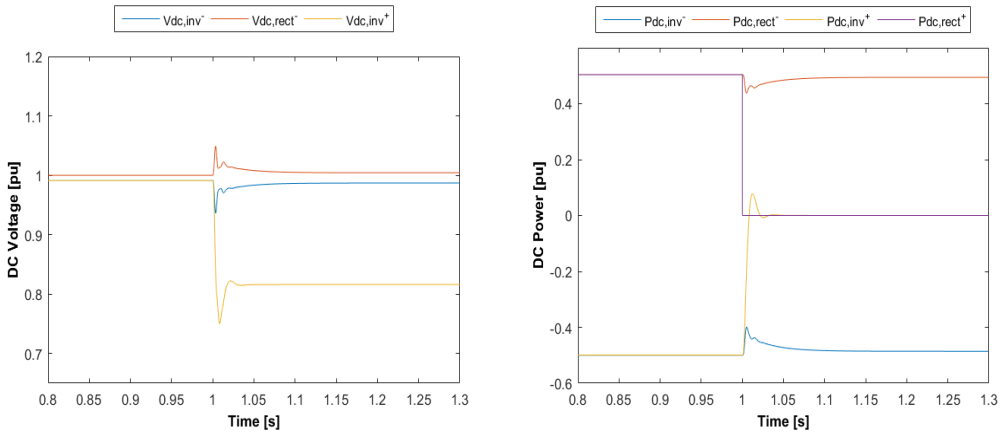

(a) DC Voltage profile

(b) Power profile

Figure 5.17: Simulation results of Rectifier+ outage, implementation of a cable model with three parallel branches.

5.4.2 Meshed bipolar grid

The second simulation is performed with a droop control on a bipolar four terminals meshed grid. The layout of the grid is shown in figure 5.18. The grid and droop control parameters can be found in table 5.4, in which only the current set-points are given since the voltage set-points coincide with the initial values listed in table 5.5.

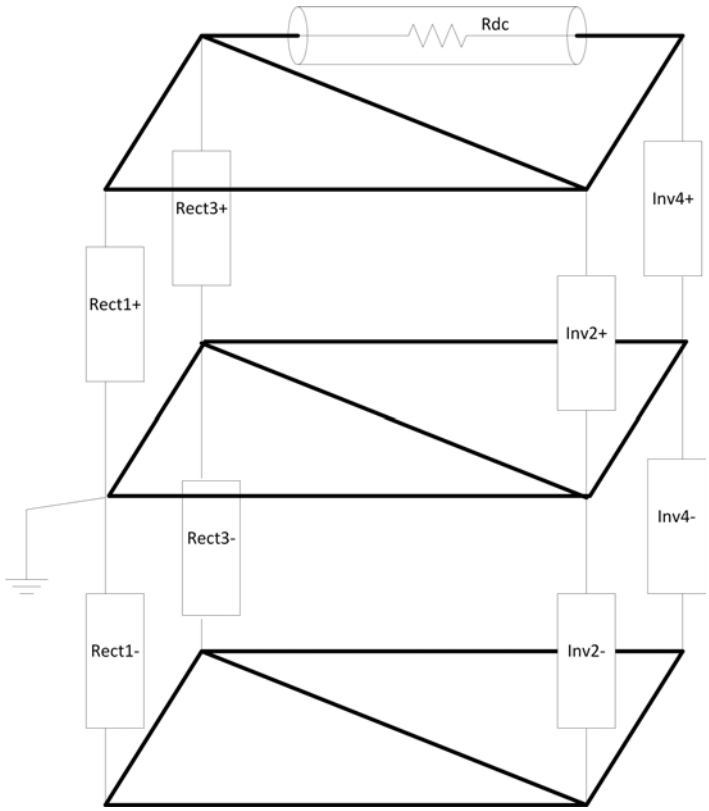

Figure 5.18: Power profile

Table 5.4: Grid and control parameters

Grid Parameters		**Droop Parameters**	
Rated Power	1200 [MW]	G_{dc} (droop gain)	9.6577
Rated Voltage	380 [kV]	$I_{dc,0}$ Rect1	0.6985 [pu]
R_{dc}	0.0351 [pu]	$I_{dc,0}$ Rect3	1.0400 [pu]
R_{dcm}	0.0351 [pu]	$I_{dc,0}$ Inv2	-0.9185 [pu]
line length	300 [km]	$I_{dc,0}$ Inv4	-0.8200 [pu]

Initially the converters at the station number 3 delivers the full rated power, 1200 MW. After one second the VSC in the third station at the positive pole has an outage and its power output becomes suddenly zero. Figures 5.19 (a) and 5.20 (a) show the power profiles for respectively the positive and the negative pole; while figures 5.19 (b) and 5.20 (b) show the voltage profiles. The voltage at every node in the positive pole decreases as a consequence of the lack of current flowing into the DC grid. The value of droop gain that is found after the tuning of the controllers allows a voltage variation of 1% with respect to a per unit change of the current. The voltage variation in the negative pole is positive at node 1, where the unbalanced current enters the metallic return. The voltage variation is negative in the other nodes where the unbalanced current leaves the return path.

Table 5.5: Simulation results of the outage of the rectifier in the positive pole

Initial Values:	**Power [pu]**	**Voltage [pu]**
Rect1+	0.7	1.0022
Inv2+	-0.9	0.9799
Rect3+	1.040	1
Inv4+	-0.8	0.9756
Rect1-	0.7	1.0022
Inv2-	-0.9	0.9799
Rect3-	1.040	1
Inv4-	-0.8	0.9756
After the contingency:	**Power [pu]**	**Voltage [pu]**
Rect1+	1.014	0.9658
Inv2+	-0.5505	0.9452
Rect3+	0	0.9383
Inv4+	-0.4394	0.9392
Rect1-	0.7236	0.9996
Inv2-	-0.8663	0.9767
Rect3-	0.9657	1.009
Inv4-	-0.7729	0.9730

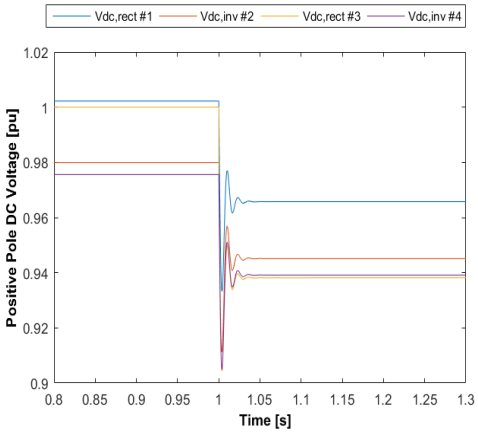

(a) Positive pole DC voltage profile

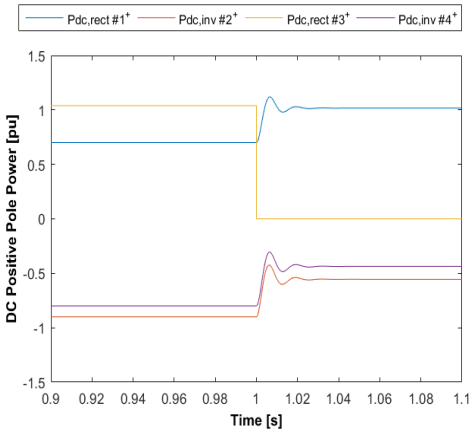

(b) Positive pole power profile

Figure 5.19: Simulation results of the outage of Rect3+ in the positive pole of a meshed MTDC grid

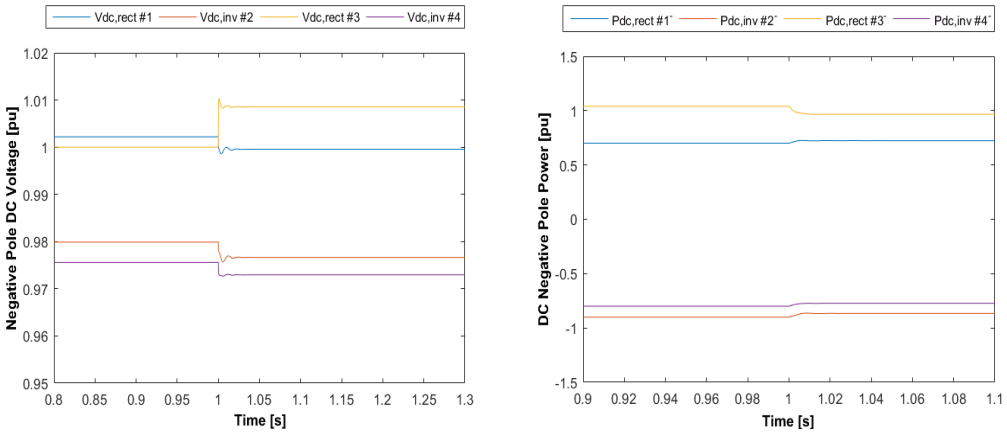

(a) Negative pole DC voltage profile

(b) Negative pole power profile

Figure 5.20: Simulation results of the outage of Rect3+ in the negative pole of a meshed MTDC grid

5.4.3 Conclusion

The control system achieves a good dynamic response and a stable operating point is quickly reached. When an outage occurs on one pole, the contribution of the droop control systems in the opposite pole to balance the power is inherently present, but remains limited. A further study could be done on the implementation of a set-points change that allows a more equal share of the unbalanced power between the converters of the positive and negative poles.

Furthermore, the analysis pointed out an interaction between the two poles as a consequence of the asymmetric outage. This interaction, defined as the degree of reaction of one pole to a contingency on the opposite pole, will be called coupling in the rest of the thesis. The next chapter investigates the dependence of the coupling between the two poles on the parameters of the VSC-HVDC grid.

Chapter 6

Converter outage in a bipolar configuration

6.1 Introduction

Whereas the previous chapter focused on the dynamic behavior of the MTDC grid after a contingency, this chapter analyses how the outage of a converter can affect the MTDC bipolar grid from a steady-state perspective. In a meshed HVDC grid, the outage of a converter causes a power mismatch and the subsequent reaction of the VSC voltage droop controllers aims at reestablishing a balanced operation. The new stable currents and voltages need to be a solution of the power flow description of the grid and a working point in the droop characteristic at every operating converter. The outage of a rectifier is a drastic lack of power injection that causes a deficit of current in the whole grid and consequently the discharge of the converter capacitances and cable capacitances. The voltage at every node decreases and the droop controllers detect this voltage variation due to a local measurement. When the converter experiencing the outage is an inverter, the power withdrawal suddenly decreases and instead, the system suffers from a surplus of current. Consequently, the voltage at every node increases.

The contribution of every converter to the power stabilization is dependent on the value of the droop gain implemented in its controller. If the droop constant is the same everywhere, all converters will take equal power share given equal voltage variation, but because of the voltage drop along the DC lines, in a real system the voltage variations are different at every terminal. To achieve an optimal operation and integration of the control strategy in the whole system, including the AC side, a good droop control design has to assign to each node a power share that takes into account multiple variables such as:

Converter ratings. The power variation at every node has to respect current limitations in order not to damage the different components of the converters.

Operating conditions. The power rating of a converter does not reflect its loading condition in a particular operating point. In [57], a variable droop control gain has been proposed so that each converter can contribute to the power sharing in respect to the available headroom, i.e. the difference between its rated capacity and the present loading.

AC and DC power flows. The outage causes the variation of all converters set-points, consequently, it will also influence the power flows in the AC side if parallel paths between DC and AC side are present and, after the control action, loop flows or instability might appear [58]. In [33], a study of the connection between power flows in the AC and DC side has been conducted showing the big impact that the voltage droop control has on both sides and the necessity of a coordinated control. Finally in [59], it was demonstrated that the droop constants can be computed in order to optimize the power distribution in the AC system after the outage.

AC and DC dynamic stability. An outage also effects also the dynamic stability of both AC

and DC sides. Transients and power oscillations on the AC side may be a consequence of the DC contingencies and an optimal design of the droop gain can damp these effects. In [58] a method using Singular Value Decomposition (SVD) has been developed with the aim of reducing the dynamic impact of DC disturbances on the AC network. In [60], a SVD technique has been implemented to design a droop control that satisfies the dynamic DC requirements.

From the steady-state point of view, the set-points of the droop controller can be adjusted in order to obtain a desired power flow. In [61] this is done using an Optimal Power Flow (OPF) algorithm ensuring loss minimization in the transmission system but with the requirement of communication between the converters. In [62] the OPF formula aims at optimizing the combined AC-DC system.

In the following sections of this chapter the effect of an asymmetric outage on a bipolar multi-terminal HVDC grid will be described. Initially, equal droop gains will be assigned to each converter of both poles as was done in [63] with the aim to analyze the transient response and the consequences of the outage on the steady-state values. This will allow to study the influence of the metallic return resistance on the coupling between the two poles.

6.2 Asymmetric outage in a bipolar MTDC grid

In a monopolar grid configuration the outage of a converter cancels out any power exchange at that node, in some cases leading to a division of the grid in two separated parts. When the meshed HVDC grid has a bipolar configuration, only the contemporary outage of both converters in a station has the same implications. With a single converter outage, asymmetric outage, the grid node can instead be operated at half of its rated power, or even more if the converter can be partially overloaded. In normal operation the current on the return path is zero because the two poles are controlled to be equal, i.e. every converter is equally loaded with respect to the converter at the opposite pole of the same node. On the contrary, an asymmetric outage causes a difference in the loading of the poles and the current on the return path is no longer equal to zero. As it has been explained in chapter 3, the return path can be the ground if there is a connection to earth between the two converters in every station, or a dedicated conductor called metallic return. The second option is most likely the better solution for a future implementation since a ground return will be hardly accepted. As an alternative, the current can return through the healthy pole conductor if the node where the outage occurs is connected radially to other nodes [14].

The two poles of a bipolar configuration can be controlled independently (separate control) or in a master/slave mode (balanced control). The independent control mode has the advantage that the power in each pole can be chosen irrespectively to the power transmitted in the other pole. With a balanced control, the outage of a converter in the upper pole will result in the lower pole at the same node to reduce its power as well, excluding that node from the grid completely. An independent operation is preferred, because the power at the node suffering the outage of a converter can still be delivered at half the rated power of that DC node by the converter in the other pole. This is even more important if the node suffering the outage is not radially connected to the other nodes and the power coming from or going into it cannot be rerouted through other paths.

With separate control, the two poles behave like independent systems, however the outage of a converter in one pole has an influence on the other pole. The power mismatch in every DC line results in a current flow in the metallic return. At every node some current is entering the neutral or exiting it. The voltage at the neutral nodes (the mid point between the converters of a station) is no longer zero, with the exception of the grounded node, and consequently a shift of the voltages is also registered in the upper pole and lower pole. The droop controllers react to a local measurement of the voltage between the terminals of each converter hence, when the voltage at the neutral point is shifting, the controllers detect a voltage variation also in the pole that is not experiencing the outage. This correlation between the positive and the negative pole results in an inherent coupling that depends, amongst others, on the resistance of the neutral system and on the value of the droop gain. By differently dimensioning the return path, the

coupling between the poles alters, in the sense that with a stronger coupling a power unbalance in one pole causes a bigger variation of the set-points in the other pole. The voltage variation at the opposite pole can be relevant (up to $2,5\%$ of the base voltage in the following simulation, i.e. $\approx 7,8$ kV). An understanding of this correlation is also important for the planning of a correct secondary control action.

6.3 Converter current sharing after the outage

The analysis developed in [64] will now be extended to a bipolar grid configuration to mathematically express the relation between droop control settings and steady-state voltage deviations and power sharing, taking into account the power flows in the DC grid. The model will be described with separate equations for the nodes in the positive pole, negative pole and neutral path.

6.3.1 Droop control and converter outage

The droop control law that is used in the following mathematical model is the current-based droop law with local voltage measurement. For the converter i the relation between current I_{DC_i} and voltage U_{DC_i} is:

$$I_{DC_i} = I_{DC,0_i} - \frac{1}{k_{DC_i}}(U_{DC_i} - U_{DC,0_i}) \tag{6.1}$$

where $I_{DC,0_i}$ is the reference value of the current and $U_{DC,0_i}$ the reference value for the voltage. These reference values can be the initial set point or alternatively any of the points in the droop characteristic.

The outage of converter i results in the sudden drop of his power/current output from the initial steady state value $I_{DC,0_i}$ to zero. It can be written as

$$\Delta I_{DC_i} = -I_{DC,0_i}. \tag{6.2}$$

The fault is followed by a rearrangement of the currents in all the other converters j implementing a droop voltage control. The droop law for the j converters is

$$\Delta I_{DC_j} = -g_j \Delta U_{DC_j} \tag{6.3}$$

where g_j is the gain of the proportional controller, defined as the inverse of the droop constant k_{DC_j}. Multiplying and dividing (6.3) with ΔI_{DC_i} and substituting (6.2) at the nominator and at the denominator the equation of current balance in the DC lines

$$\Delta I_{DC_i} = \sum_{\substack{k=1 \\ k \neq i}}^{n} \Delta I_{DC_k} = -\sum_{\substack{k=1 \\ k \neq i}}^{n} g_k \Delta U_{DC_k} \tag{6.4}$$

we obtain

$$\Delta I_{DC_j} = I_{DC,0_i} \cdot g'_j \tag{6.5}$$

where g'_j is the modified gain for converter j

$$g'_j = \frac{g_j \Delta U_{DC_j}}{\sum_{\substack{k=1 \\ k \neq i}}^{n} g_k \Delta U_{DC_k}} \tag{6.6}$$

It can be observed in equation (6.3) that the current variations at every converter depends on the voltage variation detected by the local measurement after the outage. Only in the case of a common voltage feedback the dependency does not exist since $\Delta U_{DC_j} = \Delta U_{DC_k}$ and the expression of the current shares after the fault is

$$\Delta I_{DC_j} = I_{DC,0_i} \cdot \frac{g_j}{\sum_{\substack{k=1 \\ k \neq i}}^{n} g_k} \tag{6.7}$$

6.3.2 Network equations and droop law

In this section a mathematical formula is given to integrate the droop I-V law in the DC network equations in order to study how the droop controller action effects the current sharing and voltage variation following a converter outage. To conduct the analysis on the bipolar configuration, the equations will be written for each layer of the grid: positive, neutral and negative.

Grouping all current injections and node voltages, the steady-state network equations can be written as

$$\begin{aligned} \mathsf{Y}^{+}_{\mathsf{DC}}\mathbf{U}^{+}_{\mathbf{DC}} &= \mathbf{I}^{+}_{\mathbf{DC}} \\ \mathsf{Y}^{-}_{\mathsf{DC}}\mathbf{U}^{-}_{\mathbf{DC}} &= -\mathbf{I}^{-}_{\mathbf{DC}} \\ \mathsf{Y}^{0}_{\mathsf{DC}}\mathbf{U}^{\mathbf{0}}_{\mathbf{DC}} &= \mathbf{I}^{\mathbf{0}}_{\mathbf{DC}} = -\mathbf{I}^{+}_{\mathbf{DC}} + \mathbf{I}^{-}_{\mathbf{DC}} \end{aligned} \tag{6.8}$$

where U^{+}_{DC}, U^{-}_{DC} and U^{0}_{DC} are respectively the vectors of the voltages at the DC nodes in the positive, negative and neutral subsystems; I^{+}_{DC} and I^{-}_{DC} are the vectors of the currents injected by the converters in the positive and negative poles and I^{0}_{DC} is the vector of the differential currents at the node between the two converters in each station. Finally Y^{+}_{DC}, Y^{-}_{DC} and Y^{0}_{DC} are the admittance matrices of the three DC subsystems. The current and voltage vectors can be now written as the sum of the initial value and a deviation

$$\begin{aligned} \mathbf{U}^{+}_{\mathbf{DC}} &= \mathbf{U}^{+}_{\mathbf{DC,0}} + \mathbf{\Delta U}^{+}_{\mathbf{DC}} \\ \mathbf{U}^{-}_{\mathbf{DC}} &= \mathbf{U}^{-}_{\mathbf{DC,0}} + \mathbf{\Delta U}^{-}_{\mathbf{DC}} \\ \mathbf{U}^{\mathbf{0}}_{\mathbf{DC}} &= \mathbf{U}^{\mathbf{0}}_{\mathbf{DC,0}} + \mathbf{\Delta U}^{\mathbf{0}}_{\mathbf{DC}} \end{aligned} \tag{6.9}$$

$$\begin{aligned} \mathbf{I}^{+}_{\mathbf{DC}} &= \mathbf{I}^{+}_{\mathbf{DC,0}} + \mathbf{\Delta I}^{+}_{\mathbf{DC}} \\ \mathbf{I}^{-}_{\mathbf{DC}} &= \mathbf{I}^{-}_{\mathbf{DC,0}} + \mathbf{\Delta I}^{-}_{\mathbf{DC}} \\ \mathbf{I}^{\mathbf{0}}_{\mathbf{DC}} &= \mathbf{I}^{\mathbf{0}}_{\mathbf{DC,0}} + \mathbf{\Delta I}^{\mathbf{0}}_{\mathbf{DC}}. \end{aligned} \tag{6.10}$$

Substituting these expressions in equations (6.8) gives

$$\begin{aligned} \mathbf{I}^{+}_{\mathbf{DC,0}} - \mathsf{Y}^{+}_{\mathsf{DC}}\mathbf{U}^{+}_{\mathbf{DC,0}} &= \mathsf{Y}^{+}_{\mathsf{DC}}\mathbf{\Delta U}^{+}_{\mathbf{DC}} - \mathbf{\Delta I}^{+}_{\mathbf{DC}} \\ -\mathbf{I}^{-}_{\mathbf{DC,0}} - \mathsf{Y}^{-}_{\mathsf{DC}}\mathbf{U}^{-}_{\mathbf{DC,0}} &= \mathsf{Y}^{-}_{\mathsf{DC}}\mathbf{\Delta U}^{-}_{\mathbf{DC}} + \mathbf{\Delta I}^{-}_{\mathbf{DC}} \\ \mathbf{I}^{\mathbf{0}}_{\mathbf{DC,0}} - \mathsf{Y}^{0}_{\mathsf{DC}}\mathbf{U}^{\mathbf{0}}_{\mathbf{DC,0}} &= \mathsf{Y}^{0}_{\mathsf{DC}}\mathbf{\Delta U}^{\mathbf{0}}_{\mathbf{DC}} - \mathbf{\Delta I}^{\mathbf{0}}_{\mathbf{DC}}. \end{aligned} \tag{6.11}$$

The droop law (6.1) in matrix terms looks like

$$\begin{aligned} \mathbf{\Delta I}^{+}_{\mathbf{DC}} &= -\mathsf{G}^{+}(\mathbf{\Delta U}^{+}_{\mathbf{DC}} - \mathbf{\Delta U}^{\mathbf{0}}_{\mathbf{DC}}) \\ \mathbf{\Delta I}^{-}_{\mathbf{DC}} &= -\mathsf{G}^{-}(\mathbf{\Delta U}^{\mathbf{0}}_{\mathbf{DC}} - \mathbf{\Delta U}^{-}_{\mathbf{DC}}) \end{aligned} \tag{6.12}$$

where G^{+} and G^{-} are diagonal matrices that contain the droop control gains of the converters controllers respectively for the positive pole and for the negative pole.

As $\mathbf{U_{DC,0}}$ and $\mathbf{I_{DC,0}}$ (voltages and currents before the outage) in the left hand side of the equations (6.11) can be chosen to satisfy the power flow equations (6.8), substituting (6.12) and recalling that $\mathbf{\Delta I^{0}_{DC}} = -\mathbf{\Delta I^{+}_{DC}} + \mathbf{\Delta I^{-}_{DC}}$, the relation (6.11) becomes

$$\begin{aligned} 0 &= (\mathsf{Y}^{+}_{\mathsf{DC}} + \mathsf{G}^{+})\mathbf{\Delta U}^{+}_{\mathbf{DC}} - \mathsf{G}^{+}\mathbf{\Delta U}^{\mathbf{0}}_{\mathbf{DC}} \\ 0 &= (\mathsf{Y}^{-}_{\mathsf{DC}} + \mathsf{G}^{-})\mathbf{\Delta U}^{-}_{\mathbf{DC}} - \mathsf{G}^{-}\mathbf{\Delta U}^{\mathbf{0}}_{\mathbf{DC}} \\ 0 &= (\mathsf{Y}^{0}_{\mathsf{DC}} + \mathsf{G}^{+} + \mathsf{G}^{-})\mathbf{\Delta U}^{\mathbf{0}}_{\mathbf{DC}} - \mathsf{G}^{+}\mathbf{\Delta U}^{+}_{\mathbf{DC}} - \mathsf{G}^{-}\mathbf{\Delta U}^{-}_{\mathbf{DC}} \end{aligned} \tag{6.13}$$

The absence of a converter or a bus with constant current injection can be represented similar to the outage of a converter by changing the matrix of the gains G and accordingly by adding a zero entry in the vector of the current injections $\mathbf{I_{DC,0}}$. If the outage is asymmetric and it occurs for example in the positive pole, the only matrices that have to be updated are

G^+, $\mathbf{I}^+_{\mathbf{DC,0}}$ and $\mathbf{I}^{\mathbf{0}}_{\mathbf{DC,0}}$. Similarly, when the outage occurs in the negative pole G^-, $\mathbf{I}^-_{\mathbf{DC,0}}$ and $\mathbf{I}^{\mathbf{0}}_{\mathbf{DC,0}}$ have to be updated. The modified gain matrix after the outage of converter i in the positive pole looks like

$$\mathsf{G}^+_{\mathsf{out}} = diag([g_1^+ \cdots g_{i-1}^+ \ 0 \ g_{i+1}^+ \cdots g_n^+]). \tag{6.14}$$

When, alternatively, the converter experiencing the fault is located in the negative subsystem, the matrix that has to be modified is

$$\mathsf{G}^-_{\mathsf{out}} = diag([g_1^- \cdots g_{i-1}^- \ 0 \ g_{i+1}^- \cdots g_n^-]). \tag{6.15}$$

The modified gain matrix represents the droop controllers action of changing the converters current injection after a voltage variation due to the failure of a converter in the grid.

An alternative way to study the outage is by applying the superposition principle to (6.11) and thus, accounting only for the unbalanced part, the voltage variations obtained at each grid node due to the outage of converter i in the positive pole

$$\begin{aligned} \mathbf{I}^+_{\mathbf{DC,out}} &= (\mathsf{Y}^+_{\mathsf{DC}} + \mathsf{G}^+_{\mathsf{out}})\mathbf{\Delta U}^+_{\mathbf{DC}} - \mathsf{G}^+_{\mathsf{out}}\mathbf{\Delta U}^{\mathbf{0}}_{\mathbf{DC}} \\ 0 &= (\mathsf{Y}^-_{\mathsf{DC}} + \mathsf{G}^-)\mathbf{\Delta U}^-_{\mathbf{DC}} - \mathsf{G}^-\mathbf{\Delta U}^{\mathbf{0}}_{\mathbf{DC}} \\ -\mathbf{I}^+_{\mathbf{DC,out}} &= (\mathsf{Y}^0_{\mathsf{DC}} + \mathsf{G}^+_{\mathsf{out}} + \mathsf{G}^-)\mathbf{\Delta U}^{\mathbf{0}}_{\mathbf{DC}} - \mathsf{G}^+_{\mathsf{out}}\mathbf{\Delta U}^+_{\mathbf{DC}} - \mathsf{G}^-\mathbf{\Delta U}^-_{\mathbf{DC}} \end{aligned} \tag{6.16}$$

where $\mathbf{I}^+_{\mathbf{DC,out}}$ is the current outage vector that is defined as

$$\mathbf{I}^+_{\mathbf{DC,out}} = [0 \ \cdots \ 0 \ -I_{DC,0_i} \ 0 \ \cdots \ 0]^T$$

Similarly, if the asymmetric outage of converter i occurs in the negative pole (6.16) becomes

$$\begin{aligned} 0 &= (\mathsf{Y}^+_{\mathsf{DC}} + \mathsf{G}^+)\mathbf{\Delta U}^+_{\mathbf{DC}} - \mathsf{G}^+\mathbf{\Delta U}^{\mathbf{0}}_{\mathbf{DC}} \\ -\mathbf{I}^-_{\mathbf{DC,out}} &= (\mathsf{Y}^-_{\mathsf{DC}} + \mathsf{G}^-_{\mathsf{out}})\mathbf{\Delta U}^-_{\mathbf{DC}} - \mathsf{G}^-_{\mathsf{out}}\mathbf{\Delta U}^{\mathbf{0}}_{\mathbf{DC}} \\ \mathbf{I}^-_{\mathbf{DC,out}} &= (\mathsf{Y}^0_{\mathsf{DC}} + \mathsf{G}^+ + \mathsf{G}^-_{\mathsf{out}})\mathbf{\Delta U}^{\mathbf{0}}_{\mathbf{DC}} - \mathsf{G}^+\mathbf{\Delta U}^+_{\mathbf{DC}} - \mathsf{G}^-_{\mathsf{out}}\mathbf{\Delta U}^-_{\mathbf{DC}}. \end{aligned} \tag{6.17}$$

Finally the variation of the change in injected currents is equally calculated by substituting the voltage variations in the DC subsystems equations or in the droop control relations since a new stable steady-state point has been reached

$$\begin{aligned} \mathbf{\Delta I}^+_{\mathbf{DC}} &= \mathsf{Y}^+_{\mathsf{DC}}\mathbf{\Delta U}^+_{\mathbf{DC}} &&= -\mathsf{G}^+_{\mathsf{out}}(\mathbf{\Delta U}^+_{\mathbf{DC}} - \mathbf{\Delta U}^{\mathbf{0}}_{\mathbf{DC}}) \\ \mathbf{\Delta I}^-_{\mathbf{DC}} &= -\mathsf{Y}^-_{\mathsf{DC}}\mathbf{\Delta U}^-_{\mathbf{DC}} &&= -\mathsf{G}^-(\mathbf{\Delta U}^{\mathbf{0}}_{\mathbf{DC}} - \mathbf{\Delta U}^-_{\mathbf{DC}}) \end{aligned} \tag{6.18}$$

for the outage of a positive pole converter and

$$\begin{aligned} \mathbf{\Delta I}^+_{\mathbf{DC}} &= \mathsf{Y}^+_{\mathsf{DC}}\mathbf{\Delta U}^+_{\mathbf{DC}} &&= -\mathsf{G}^+(\mathbf{\Delta U}^+_{\mathbf{DC}} - \mathbf{\Delta U}^{\mathbf{0}}_{\mathbf{DC}}) \\ \mathbf{\Delta I}^-_{\mathbf{DC}} &= -\mathsf{Y}^-_{\mathsf{DC}}\mathbf{\Delta U}^-_{\mathbf{DC}} &&= -\mathsf{G}^-_{\mathsf{out}}(\mathbf{\Delta U}^{\mathbf{0}}_{\mathbf{DC}} - \mathbf{\Delta U}^-_{\mathbf{DC}}) \end{aligned} \tag{6.19}$$

for the outage of a converter in the negative subsystem.

The equations described above can be represented in an electrical model. In fact, mathematically adding the modified gain diagonal matrix to the admittance matrix can be considered equivalent to define a new modified admittance matrix that includes the droop constants as resistances

$$\mathsf{Y}'^+_{\mathsf{DC}} = \mathsf{Y}^+_{\mathsf{DC}} + \mathsf{G}^+_{\mathsf{out}} \tag{6.20}$$

$$\mathsf{Y}'^-_{\mathsf{DC}} = \mathsf{Y}^-_{\mathsf{DC}} + \mathsf{G}^-_{\mathsf{out}}. \tag{6.21}$$

In figure 6.1 the equivalent bipolar electrical model is depicted and the resistances representing the droop control action are connected between the poles and the return path.

The outage of converter three in the grid of figure 6.1 is electrically modeled as a negative current injection, hence a current source connected between the node suffering the fault and the return path as depicted in figure 6.2.

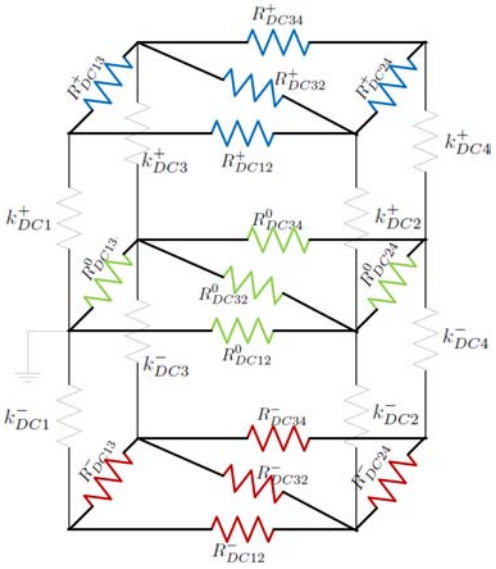

Figure 6.1: Electrical equivalent model of the bipolar grid with droop control

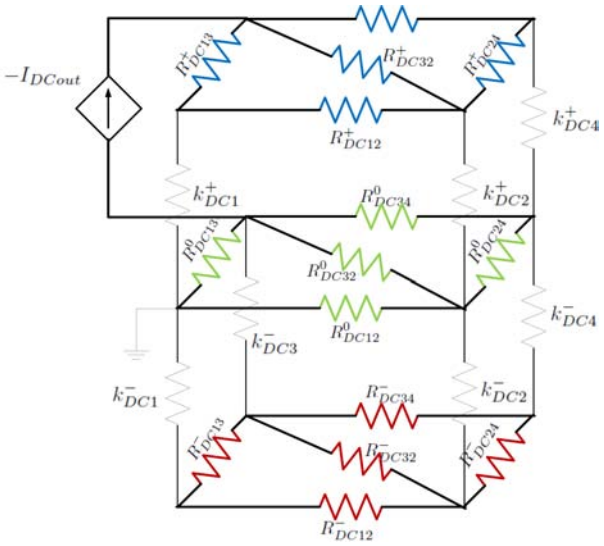

Figure 6.2: Electrical equivalent model of the bipolar grid and the outage of a converter in the positive pole.

6.4 Parameters which influence the coupling between poles

From the simulations of an asymmetric outage performed on a bipolar configuration, an electrical coupling that relates the two poles has been noticed. This coupling is defined as the degree to which one pole compensates the unbalance caused by a contingency in the opposite pole. Two quantities used to study this reaction are DC voltage and power variation. In fact, in a bipolar configuration with only one node grounded, the pole not suffering the outage is not completely independent from the other one. On the contrary, both poles see a voltage variation at their terminals and thus the droop control law implies a change of the power settings in all converters. If instead the grid is (ideally) grounded at every node the two poles behave as completely decoupled systems. It is interesting to understand which parameters influence the coupling and to which extent they affect it. The mathematical description of the outage given in the previous section allows to analyze the influence of the grid parameters, such as return path resistance, line lengths and droop gain. To mathematically model the bipolar grid grounded at one station, it is necessary to constrain the voltage at that node to zero. This is done by eliminating the row and column related to that node in the modified admittance matrix of the total grid as it is demonstrated by the Kron's reduction [65].

The simulations are performed on the grid of figure 6.3, that initially works in balanced conditions and, at t=1 [s], the rectifier *Rect3+* has an outage. As explained before, the asym-

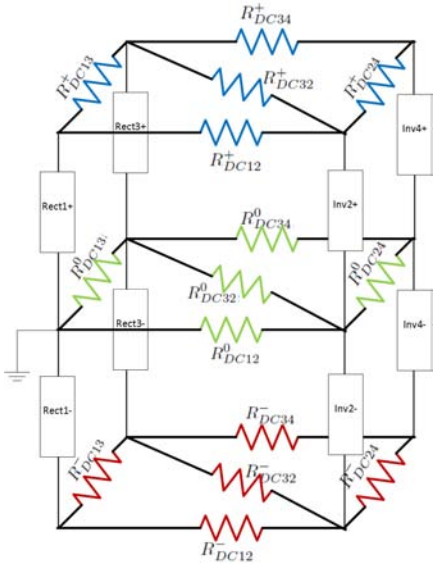

Figure 6.3: Electrical equivalent model of the bipolar grid and the outage of a converter in the positive pole.

metric fault causes an unbalanced operation of the two poles and thus a current flows in the metallic return conductor causing an offset of the voltage at the neutral and negative nodes. Therefore, all the converter droop controllers detect a DC voltage variation and react with a change of the power output. The extent to which the negative pole reacts is investigated next.

6.4.1 Metallic return resistance

The value of the return path resistance per lenght (here indicated as R_{dcm}) is one of the parameters influencing the coupling. As explained in chapter 3, in many countries a continuous earth current flow is not approved, which is why the simulations are performed on a bipolar grid with metallic return conductor grounded at one node. The metallic return layer is only grounded at a single node in order not to give a parallel earth return path to the unbalanced current.

Table 6.1 contains the values of the grid parameters and the initial working conditions of the grid converters, equal to the set-point in the droop controllers. The initial steady-state power

flow calculation can be found in Appendix A.

Table 6.1: Grid and control parameters

Grid Parameters		**Initial conditions**		
Rated Power	1200 [MW]		DC Voltage[pu]	Power [pu]
Rated Voltage	380 [kV]	Rect1+, Rect1-	1.0022	0.7
Gdc (droop gain)	9.6577	Inv2+, Inv2-	0.9799	-0.9
$Rdc_{12,13,24,34}$	0.0351 [pu]	Rect3+, Rect3-	1	1.040
Rdc_{32}	0.0496 [pu]	Inv4+, Inv4-	0.9756	-0.8
lines length(1-2,1-3,2-4,3-4)	300 [km]			
line length(3-2)	424.26 [km]			

The outage of rectifier *Rect3+* is then simulated while changing the resistance per length of the metallic return from zero to a high value in order to investigate the limits of the degree of coupling. The results are presented in figure 6.4 where there is the return conductor resistance per length in logarithmic scale on the x-axis and on the y-axis the aggregated voltage variations at the positive, neutral and negative poles; defined as:

$$\Delta Udc^{+} = \sqrt{\frac{1}{4}\sum_{k=1}^{4}(\mathbf{\Delta U_{DC}^{+}})^2} \tag{6.22}$$

$$\Delta Udc^{-} = \sqrt{\frac{1}{4}\sum_{k=1}^{4}(\mathbf{\Delta U_{DC}^{-}})^2} \tag{6.23}$$

$$\Delta Udc^{0} = \sqrt{\frac{1}{3}\sum_{k=2}^{4}(\mathbf{\Delta U_{DC}^{0}})^2} \tag{6.24}$$

In accordance with data from cables producers [66], the highlighted area in the graph indicates realistic values for the metallic return resistance. In fact $R_{dcm_{min}}$ is chosen with respect to the maximum diameter of commercialized cables and $R_{dcm_{max}}$ is the resistance of the smallest cable capable of carrying the unbalanced current. The choice of the metallic return size, and thus of its resistance, is influenced by the current that is expected to carry. When a redispatch action is implemented after the outage with the aim of limiting the unbalance, only a small current flows in the metallic return. Hence, the cable could be dimensioned smaller. When instead the cable is dimensioned for the full-load current capability, its diameter is larger and the resistance lower. Figure 6.5 shows an example of a producer's table listing the parameters of cables with increasing diameter.

In figure 6.4, it is possible to see how, after the outage, the variation of the voltage in the neutral and negative nodes increases when the resistance value increases too, tending theoretically to a perfect coupling that corresponds to a balanced situation. The limit for $R_{dcm} \to \infty$ is not investigated because it corresponds to not having a return path for the current. The other limit for $R_{dcm} = 0$ gives a perfect decoupling, i.e.

$$\Delta Udc^{-} = 0 \tag{6.25}$$

$$\Delta Udc^{0} = 0. \tag{6.26}$$

It also corresponds to the grid with perfect grounding at every node (not taking into account the actual ground resistance), hence to the completely independence of the two poles. Whatever contingency exists on one pole it does not affect the other. In this limit case equations (6.16) become simply

$$\mathbf{I_{DC,out}^{+}} = (\mathsf{Y_{DC}^{+}} + \mathsf{G_{out}^{+}})\mathbf{\Delta U_{DC}^{+}}$$

$$-\mathbf{I_{DC,out}^{+}} = -\mathsf{G_{out}^{+}}\mathbf{\Delta U_{DC}^{+}}$$

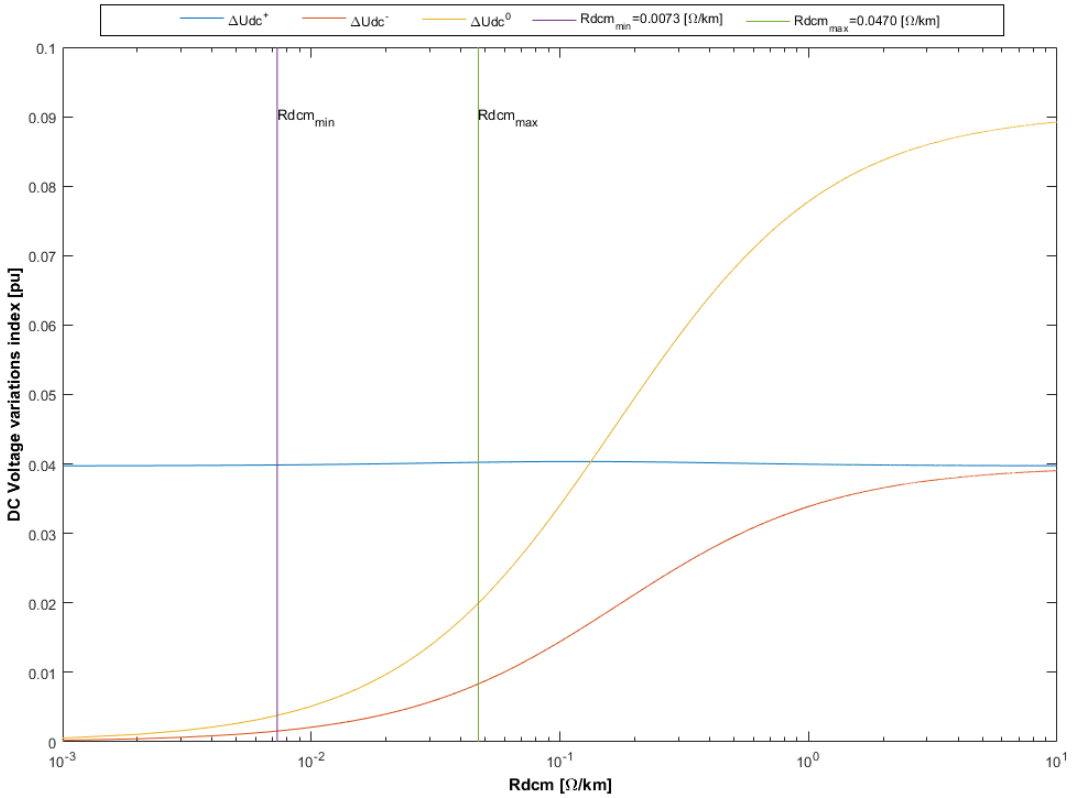

Figure 6.4: Simulation result of the metallic return resistance influence on the DC voltage

Submarine cables

Tropical climate, submarine cables with copper conductor

Area	Ampacity		±320 kV bipole				Area	Resistance
Con-ductor	Close laying	Spaced laying	Close laying	Spaced laying	Weight per cable	Diam. over cable	Copper Conductor	per phase 20 deg.C
mm²	Amps	Amps	MW	MW	kg/m	mm	mm²	ohm/km
95	282	338	180	216	15	90	95	0,193
120	323	387	207	248	16	91	120	0,153
150	363	436	232	279	17	93	150	0,124
185	411	496	263	317	18	95	185	0,0991
240	478	580	306	371	20	99	240	0,0754
300	544	662	348	424	22	102	300	0,0601
400	626	765	401	490	24	105	400	0,0470
500	722	887	462	568	26	108	500	0,0366
630	835	1030	534	659	30	114	630	0,0283
800	960	1187	614	760	33	118	800	0,0221
1000	1092	1355	699	867	37	122	1000	0,0176
1200	1188	1474	760	943	40	126	1200	0,0151
1400	1297	1614	830	1033	43	130	1400	0,0126
1600	1397	1745	894	1117	47	133	1600	0,0113
1800	1490	1860	954	1190	50	137	1800	0,0098
2000	1589	1987	1017	1272	53	140	2000	0,0090
2200	1676	2086	1073	1335	58	145	2200	0,0080
2400	1764	2198	1129	1407	61	148	2400	0,0073

Sea soil: Temperature 28 degrees C, burial 1.0 meter, thermal resistivity 1.2 K × W /m
Cable: Copper conductor, HVDC polymer insulation, steel wire armor

Figure 6.5: Capability, losses etc for submarine cables installed in moderate climate zones [66]

corresponding to the expressions derived for a monopolar configuration from [64].

Figure 6.6 shows instead the variation of the power output at the grid converters. Also in this representation the y-axis quantities are aggregated variables of the power variations at the positive and negative converters:

$$\Delta Pdc^{+} = \sqrt{\frac{1}{3}\sum_{k=1,k\neq 3}^{4}(\mathbf{\Delta P^{+}_{DC}})^2} \tag{6.27}$$

$$\Delta Pdc^{-} = \sqrt{\frac{1}{4}\sum_{k=1}^{4}(\mathbf{\Delta P^{-}_{DC}})^2} \tag{6.28}$$

$$\tag{6.29}$$

thus not accounting for the power variation in the positive pole of the converter experiencing the outage since it is not a modification due to the droop control system. The power variation at the negative pole with respect to the return resistance follows the same profile as the voltage variation, approaching the positive power output variation with an increase in R_{dcm}.

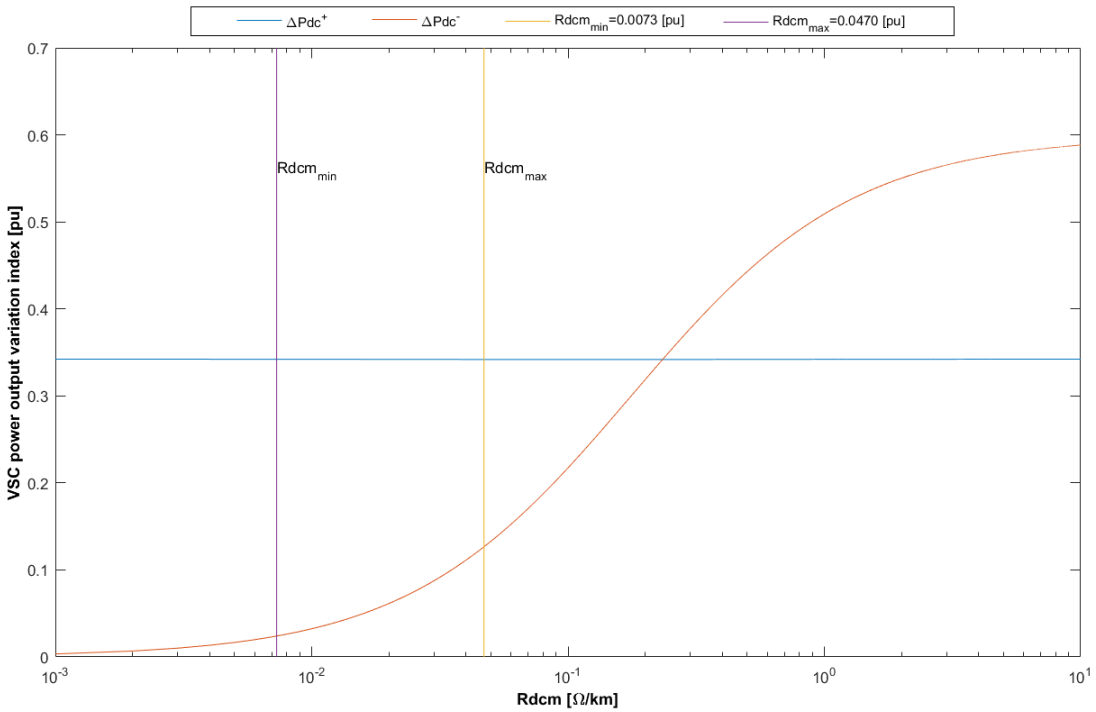

Figure 6.6: Simulation result of the metallic return resistance influence on the converters power

In the existing bipolar point-to-point HVDC links, after the outage of a VSC, the healthy pole cable is usually used as metallic return path, hence the resistance R_{dcm} is equal to the pole cable resistance placed in the middle of the area in the graph delimited by $R_{dcm_{min}}$ and $R_{dcm_{max}}$. Figure 6.7 shows how this operation mode is achieved. During balanced conditions the switches in the transversal connection between the two poles are closed. Imagine now that the rectifier of the positive pole has an outage, the switches transversally connecting the two poles are closed and the current can flow back through the positive pole cable that is correctly functioning. In a multi-terminal meshed grid every node of the grid should be connected transversally in order to avoid current flowing in the metallic return, requiring a communication system and limiting in this way the power capability and thus eliminating the biggest advantage of the bipolar configuration.

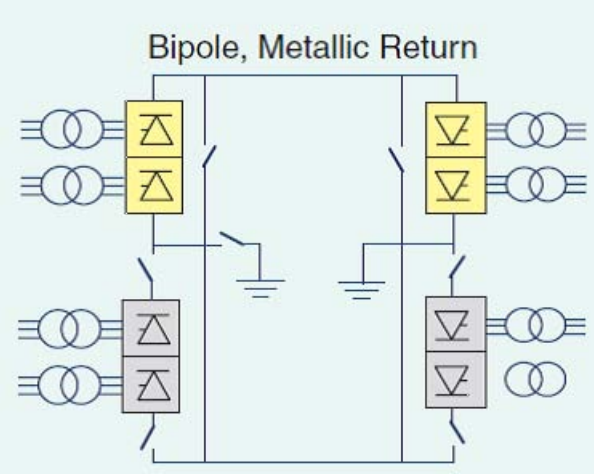

Figure 6.7: Bipolar two terminals configuration with metallic return [19]

6.4.2 Line length

The same simulation of the previous section is now performed for a fixed value of the resistance per length R_{dcm} whilst varying the length of the grid lines L. The case $L = 0$ has not been considered since the modified admittance matrix would be singular and a solution cannot be found. In accordance with [13] that lists the existing or planned VSC-HVDC projects, the chosen minimum lines length is 10 km, the maximum is 950 km. The analysis is then repeated for different values of the metallic return resistance. In particular figure 6.8 (a) depicts the voltage variation with the metallic return resistance equal to the one of the poles cables, whereas figure 6.8 (b) has $R_{dcm} = R_{dcm_{max}} = 0.0470$ [pu]. Figure 6.9 shows the converter power output variations. It can be seen that the coupling does not change substantially with the lines length,

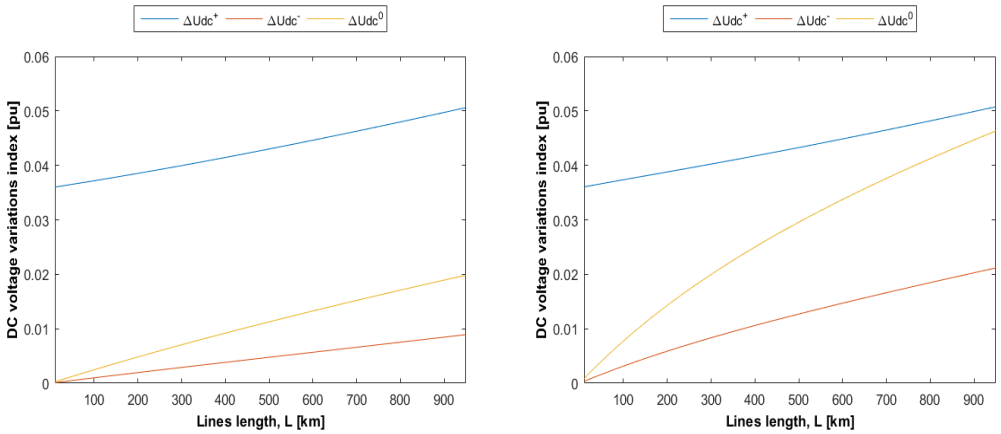

(a) $R_{dcm} = R_{dc}$ (b) $R_{dcm} = R_{dcm_{max}}$

Figure 6.8: Dependence of poles coupling on lines length, voltage variations

in figure 6.8 (b) is even constant. The voltage variation in fact increases to the same extent with the increase of the lines length. This is because the ΔUdc is partially dependent on the voltage drop on the cable resistance that increases with the length.

Once again the coupling is much more influenced by the value of the metallic return resistance as it can be seen in the limit cases of figures 6.10 (a) and (b). A very low value of the metallic return resistance gives a complete decoupling no matter the length of the lines, a high value gives complete coupling.

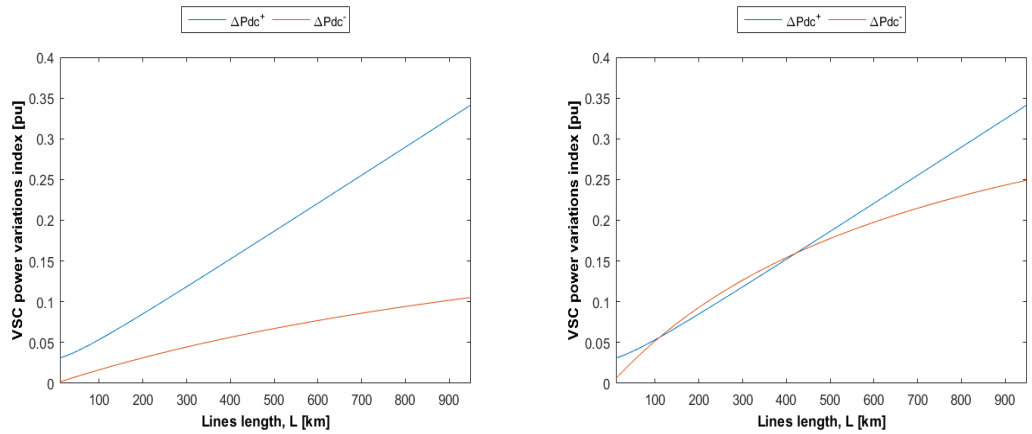

(a) $R_{dcm} = R_{dc}$ (b) $R_{dcm} = R_{dcm_{max}}$

Figure 6.9: Dependence of poles coupling on lines length, power variations

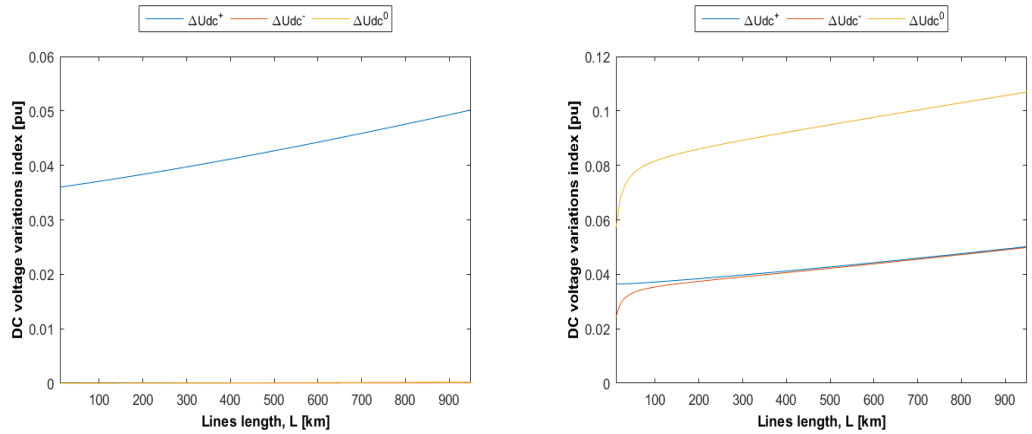

(a) $R_{dcm} = 0.0001$ (b) $R_{dcm} = 10$

Figure 6.10: Dependence of poles coupling on lines length; Rdcm limits investigation. Voltage variations.

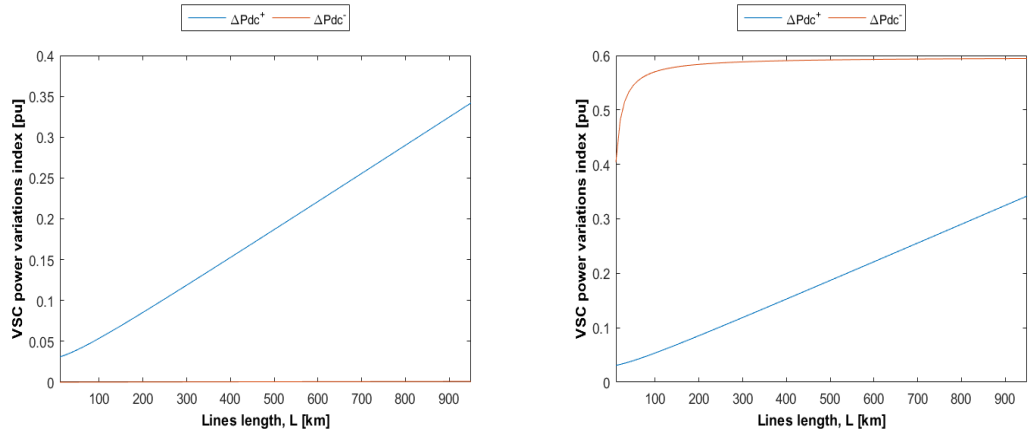

(a) $R_{dcm} = 0.0001$ (b) $R_{dcm} = 10$

Figure 6.11: Dependence of poles coupling on lines length; Rdcm limits investigation. Power variations.

6.4.3 Droop gain

The droop gain is responsible for limiting the voltage variation after an outage. In this section it is investigated to what extent it has an influence on the reaction of the negative pole to the outage in the positive one. The droop gain, equal for all the converters in the grid, is varied between 5 and 50 (giving respectively a 20% and 2% allowed voltage variation). The simulation is then repeated for different values of the return conductor resistance. Figures 6.12 and 6.14 show corresponding voltage variation in the positive, negative and neutral poles, with the droop gain scaled with respect to the reference value of $g^* = 9.66$. Figures 6.13 and 6.15 show the corresponding power variations at the VSCs. With a higher value of the droop gain the coupling increases, but not because the reaction of the negative pole has increased. It increases because the voltage variation in the positive pole, the one that faces the converter outage, decreases substantially. A very high value of the metallic return resistance implies also in this case a perfect coupling. The droop gain is now kept constant in the positive pole converters and

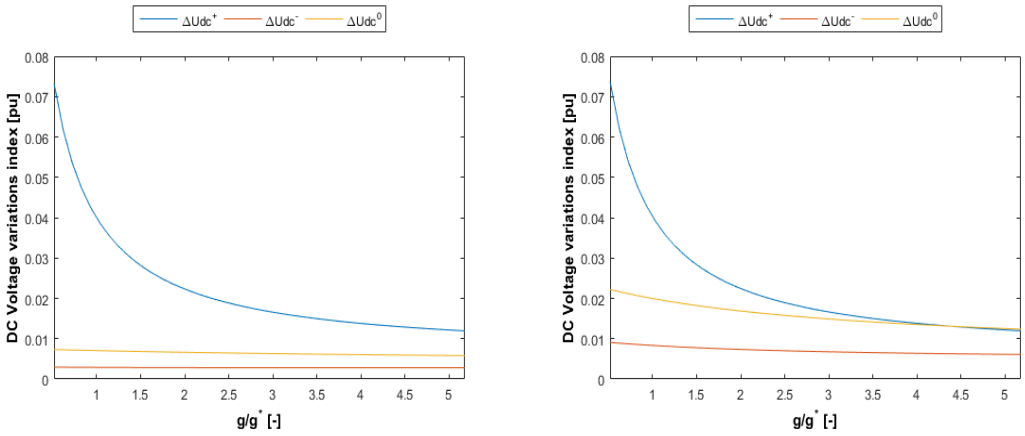

(a) $R_{dcm} = R_{dc}$ (b) $R_{dcm} = R_{dcm_{max}}$

Figure 6.12: Dependence of poles coupling on droop gain variation, voltage variations

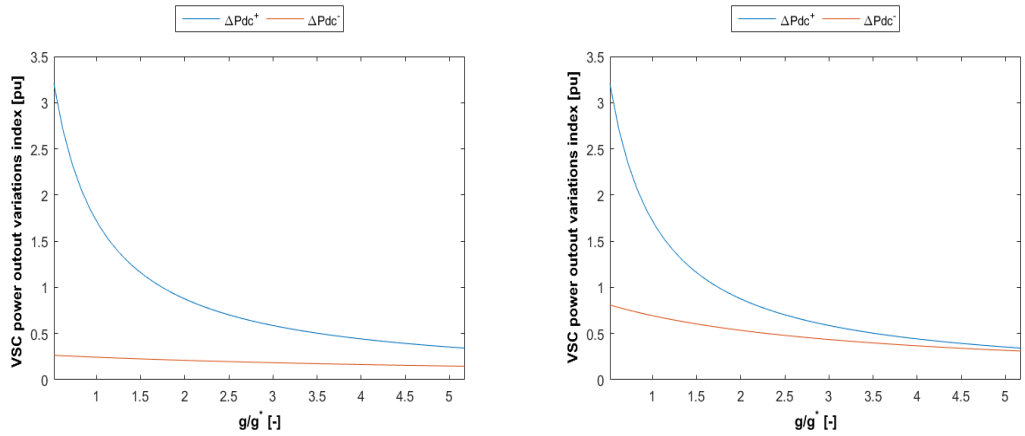

(a) $R_{dcm} = R_{dc}$ (b) $R_{dcm} = R_{dcm_{max}}$

Figure 6.13: Dependence of poles coupling on droop gain variation, power variations

varied in the same range of value as before for the converters in the negative pole. It can be seen from the comparison of figure 6.16 (a) and (b) that for a higher value of the metallic return resistance, the choice of a low droop gain in the negative pole converters increases the coupling, arriving at a complete control of the voltage variation in the negative pole when the metallic return resistance is at the highest value considered, figure 6.18 (b). However, the power

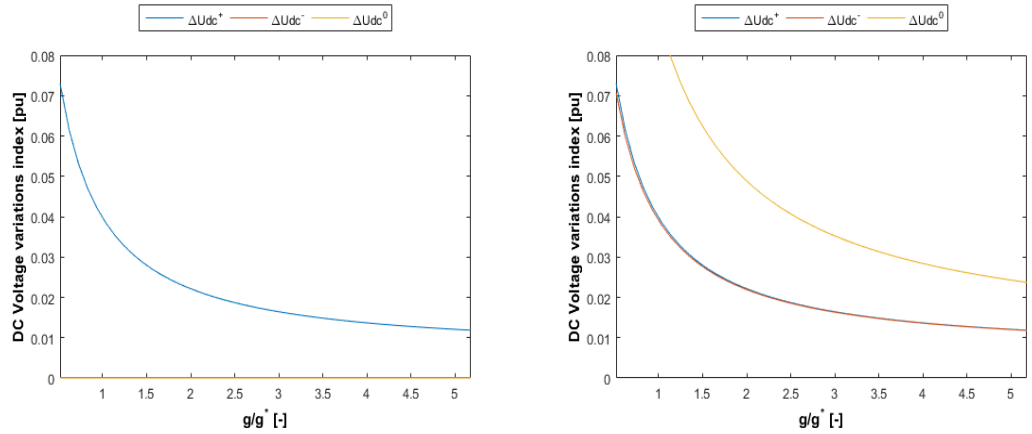

(a) $R_{dcm} = 0.0001$ (b) $R_{dcm} = 10$

Figure 6.14: Dependence of poles coupling on droop gain variation; Voltage variations. Rdcm limits investigation.

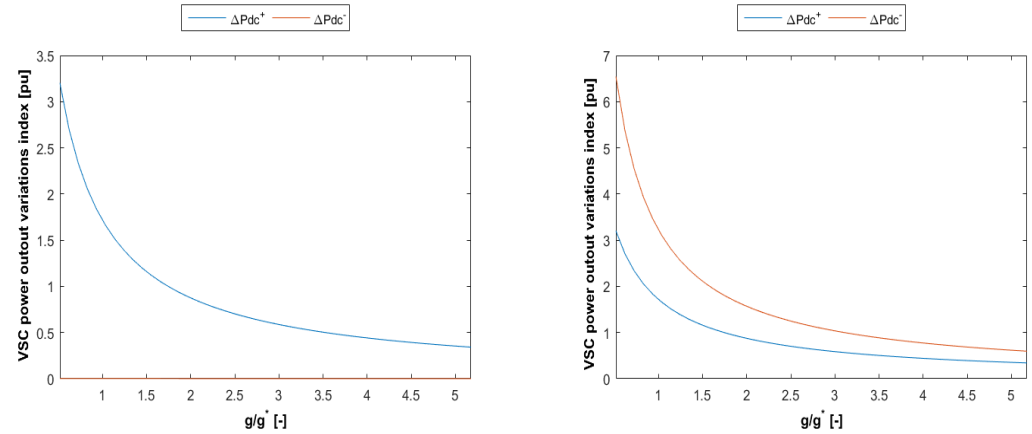

(a) $R_{dcm} = 0.0001$ (b) $R_{dcm} = 10$

Figure 6.15: Dependence of poles coupling on droop gain variation, power variation; Rdcm limits investigation. Power variations

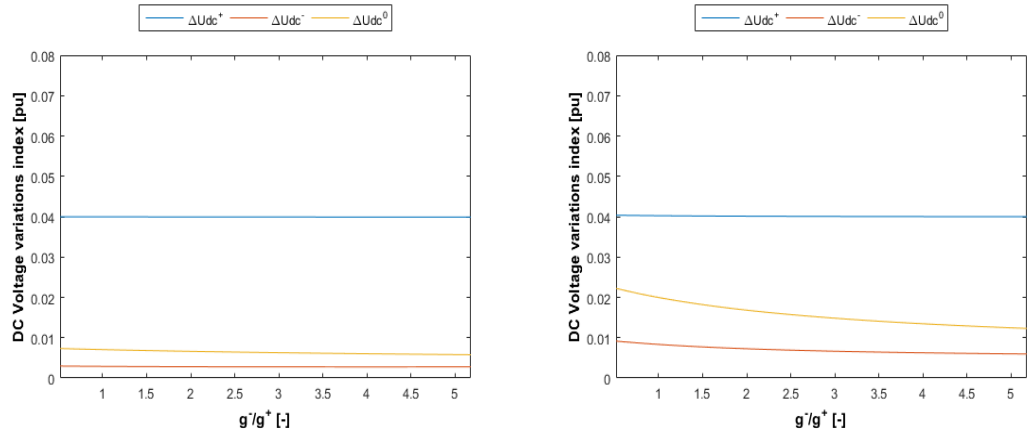

(a) $R_{dcm} = R_{dc}$ (b) $R_{dcm} = R_{dcm_{max}}$

Figure 6.16: Dependence of poles coupling on negative pole droop gain variation

variation profiles of figures 6.17 and 6.19 show that a bigger control of the coupling by changing the droop gain of the negative pole controllers, is possible only with a big variation of the power output at the grid terminals. The results for the variation of the only positive droop gain are not shown since it is an operation that does not affect the reaction of the negative pole which remains constant and changes only as a function of the resistance of the metallic return.

6.5 Conclusion

In this chapter the mathematical description of the power sharing among the different converters after an outage has been derived for a bipolar multi-terminal configuration. The electrical coupling between the two poles has been analyzed and simulations have been performed to study the influence of the grid parameters (metallic return resistance, lines length and droop gain) on the coupling. A larger value of the metallic return resistance implies a bigger variation of the voltages and currents at the terminals of the pole that is not affected by the outage. The line lengths do not substantially influence the coupling. In fact by increasing the lines length, the resistance increases equally in every DC line. Finally, by changing the value of the droop gain, the control obtained on the coupling is very limited and depends also on the value of the metallic return resistance that is the parameter that affects the coupling the most.

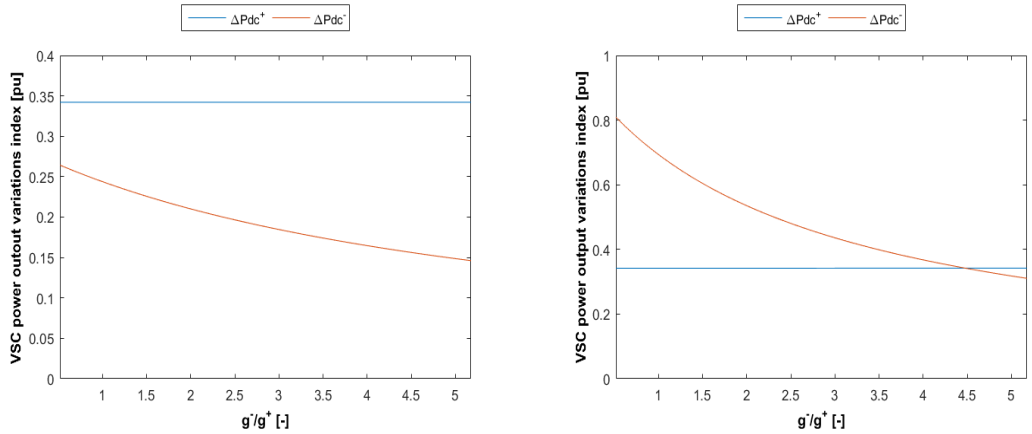

(a) $R_{dcm} = R_{dc}$ (b) $R_{dcm} = R_{dcm_{max}}$

Figure 6.17: Dependence of poles coupling on negative pole droop gain variation; power deviation

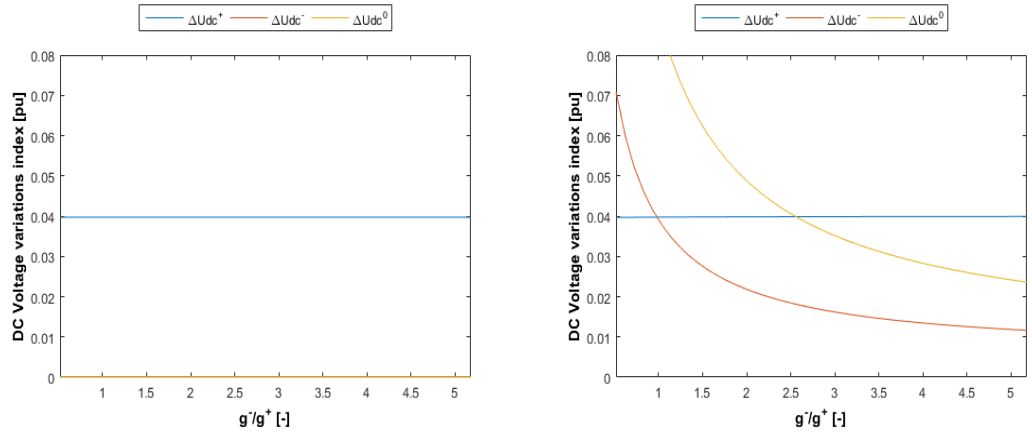

(a) $R_{dcm} = 0.0001$ (b) $R_{dcm} = 10$

Figure 6.18: Dependence of poles coupling on negative pole droop gain variation; Rdcm limits investigation.

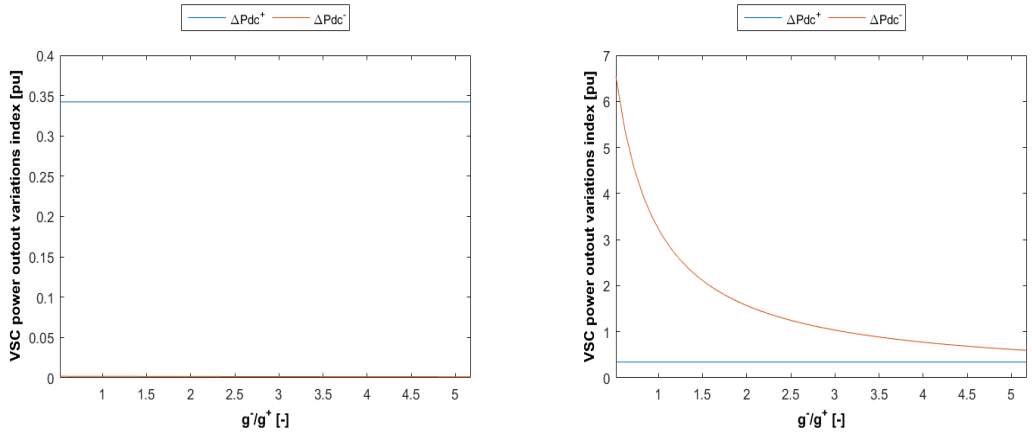

(a) $R_{dcm} = 0.0001$ (b) $R_{dcm} = 10$

Figure 6.19: Dependence of poles coupling on negative pole droop gain variation; Rdcm limits investigation. Power deviation.

Chapter 7

Conclusion

In the future development of the electricity grid, VSC-HVDC technology is expected to play a fundamental role. The existing point-to-point links might increase in number, but a meshed multi-terminal network is the solution that assures a more reliable and secure system. While the majority of the existing VSC-HVDC links use a monopolar configuration, the bipolar layout is particularly interesting for building a meshed grid since it allows the transmission of twice the power and a bigger flexibility in case of contingencies.

This thesis is a contribution on the study of the dynamical and steady-state behavior of the DC voltage control system in a bipolar multi-terminal VSC-HVDC grid.

In chapter four, the voltage control strategies, centralized and distributed, have been analyzed and compared. Firstly the constant voltage, constant power controllers have been applied in an asymmetrical three-terminal VSC-HVDC grid and the dynamic behavior after the outage of a converter has been analyzed. A stable operating point was reached by the control system, but the high requirements and limitations on the DC voltage controlling terminal decreased the reliability of the system. In fact, the VSC with a constant DC voltage control is the only converter responsible of the compensation of the unbalanced power. After a fault, the power unbalance in an extended network can be very substantial, causing a severe stress at the AC side of the controlling terminal or even causing the failure of the voltage control action if the available power headroom is not sufficient. In comparison, the droop control system (i.e. distributed control) was implemented in the same operative conditions and this strategy is better suited for the use in a multi-terminal HVDC network. In fact, all the converters in the grid contribute to the control of the voltage and after a contingency they change their power output to compensate for the unbalance.

In chapter five, the model of a bipolar HVDC grid and of the droop control system have been described. The model was implemented in MATLAB Simulink in order to validate it and to test the dynamic behavior after the asymmetric outage of a converter. The network on which the simulations were performed is a four-terminal meshed bipolar VSC-HVDC grid. A stable operating point was reached and the steady-state result pointed out a coupling between the two poles of the bipolar grid. The coupling is expressed as the degree to which one pole compensates the unbalance caused by a contingency in the opposite pole. A positive DC voltage variation manifests at the terminals of the pole not experiencing the outage where the current enters the return path, a negative variation where the current leaves the return path. Consequently, the droop controllers react and change the power output of the VSC in the pole not affected by the outage. Thus, the operation of the two poles is not independent and a possible secondary control action has to take into account the steady-state variation of the operating point of both poles.

Finally in chapter six, a mathematical analysis, describing the power sharing among converters after an outage, has been developed for the bipolar configuration. The formulation has been applied to a four-terminal bipolar network, in order to analyze the coupling between the two poles after an outage and its dependence on the grid parameters such as metallic return resistance, lines length and droop gain. The results pointed out the influence of the metallic return resistance on the size of the coupling. A smaller sized metallic return path with a higher

value for the resistance increases the voltage and power variation at the pole not experiencing the outage, tending to perfect coupling, that implies balanced operation (no current flowing in return path). On the contrary, a small value of the resistance decreases the reaction, tending to a perfect decoupling when the metallic return resistance is zero (ideal grounding at each grid terminal). The coupling does not change substantially with the line length. The voltage variation in fact increases to the same extent with the increasing of the lines length. Also the value of the droop gain has an influence. In particular, with a small droop gain in the VSC on the pole not experiencing the outage, the coupling results strengthened. On the contrary, the variation of the droop gain in the other pole does not have any influence on the degree of coupling experienced by the two poles of the bipolar network.

Acknowledgements

I would like to thank my promotors, Prof. Roberto Benato and prof. Dirk Van Hertem, who gave me the opportunity to do this research experience abroad. My gratitude also goes particularly to my daily supervisor Dr. Jef Beerten for the guidance during the course of the project. Thanks to all the PhD students that worked around me every day for making me feel welcome in Leuven and for answering to my questions. My sincere gratitude also goes to my family for the support received during these years.

Bibliography

[1] "NASA, Climate Change and Global Warming," (Last accessed: 13/03/2016). [Online]. Available: http://climate.nasa.gov/

[2] "Council of the European Union - Energy/climate change, elements of the final compromise," Brussels, 12 Dec. 2008, 17215/08.

[3] "European Commission, Communication from the commission to the European parliament, the council, the European economic and social committee of the regions - A policy framework for climate and energy in the period from 2020 to 2030," Jan. 28 2014, COM(2014) 15 final/2.

[4] "European Climate Foundation, Roadmap 2050 - A practical guide to a prosperous, low carbon europe." (Last accessed: 13/04/2016). [Online]. Available: http://www.roadmap2050.eu/

[5] "The European Wind Energy Association (EWEA), Wind in power, 2015 European statistics," Feb. 2016, last accessed: 15/04/2016. [Online]. Available: http://www.ewea.org/fileadmin/files/library/publications/statistics/EWEA-Annual-Statistics-2015.pdf

[6] D. Van Hertem and M. Ghandhari, "Multi-terminal VSC HVDC for the European supergrid: Obstacles," *Renewable Sustainable Energy Rev.*, vol. 14, no. 9, pp. 3156–3163, Dec. 2010.

[7] "European Commission, Communication from the commission to the European parliament and the council - Achieving the 10target - Making Europe's electricity grid fit for 2020," Feb. 25 2015, COM(2015) 82 final.

[8] A. Purvins, H. Wilkening, G. Fulli, E. Tzimas, G. Celli, S. Mocci, F. Pilo, and S. Tedde, "A European supergrid for renewable energy: local impacts and far-reaching challenges," *J. Cleaner Prod.*, vol. 19, no. 17-18, pp. 1909–1916, Nov.-Dec. 2011.

[9] D. Van Hertem, M. Ghandhari, and M. Delimar, "Technical limitations towards a SuperGrid. an European prospective," in *IEEE International Energy Conference and Exhibition (EnergyCon)*. Manama, 18-22 Dec. 2010, pp. 302–309.

[10] S. Gordon, "Supergrid to the rescue," *Power Eng.*, vol. 20, no. 5, pp. 30–33, Oct.-Nov. 2006.

[11] E. W. Kimbark, *Direct current transmission*. United States of America, John Wiley & Sons, 1971.

[12] E. N. of Transmission System Operators for Electricity (ENTSO-E), "Ten year network development plan 2014," 2014, (Last accessed: 07/04/2016). [Online]. Available: https://www.entsoe.eu/major-projects/ten-year-network-development-plan/Pages/index.html

[13] "School of Electrical & Electronic Engineering - University of Manchester, VSC-HVDC NEWSLETTER," Vol. 4, Issue 2, Feb. 2016.

[14] "CIGRÉ Working Group B4-52, HVDC grid feasibility study," Final Report, Dec. 2012.

[15] N. Chaudhuri, B. Chaudhuri, R. Majumder, and A. Yazdani, *Multi-terminal Direct-current Grids: Modeling, Analysis, and Control*. United States of America, John Wiley & Sons, 2014.

[16] "The European Wind Energy Association (EWEA), Oceans of opportunities - Harnessing Europe's largest domestic energy resource - A report by the EWEA," Sep. 2009.

[17] U. Lamm, "Mercury-arc valves for high-voltage dc transmission," *Proc. Inst. Electr. Eng.*, vol. 111, no. 10, pp. 1747–1753, Oct. 1964.

[18] ABB, "Product catalog 2016. Power semiconductors," 2016, (Last accessed: 15/04/2016). [Online]. Available: https://library.e.abb.com/public/28e005ea59ce4b358263b2c5c50b7682/ABB_PC2016_Web-E-Catalog.pdf

[19] M. Bahrman and B. Johnson, "The ABCs of HVDC transmission technologies," *IEEE Power Energy Mag.*, vol. 2, no. 5, pp. 32–44, 2007.

[20] L. Zhang, "Modeling and control of VSC-HVDC links connected to weak AC systems," 2010.

[21] J. Beerten, "Modeling and control of DC grids," *Ph. D. dissertation, University of Leuven (KU Leuven)*, May 2013, Leuven, Belgium.

[22] B. R. Andersen and L. Xu, "Hybrid HVDC system for power transmission to island networks," in *Transmission and Distribution Conference and Exposition, IEEE PES*, vol. 1, 2003, pp. 55–60.

[23] N. Ahmed, S. Norrga, H.-P. Nee, A. Haider, D. Van Hertem, L. Zhang, and L. Harnefors, "HVDC SuperGrids with modular multilevel converters. the power transmission backbone of the future," in *9th International Multi-Conference on Systems, Signals and Devices (SSD),*. Chemnitz, 20-23 March 2012, pp. 1–7.

[24] R. Marquardt, "Modular Multilevel Converter: An universal concept for HVDC-networks and extended DC-bus-applications," in *International Power Electronics Conference (IPEC),*. Sapporo, 21-24 June 2010, pp. 502–507.

[25] TERNA, "COLLEGAMENTO HVDC ITALIA FRANCIA denominato Piemonte - Savoia variante localizzativa tra i comuni di Bussoleno e Salbertrand al progetto autorizzato con decreto del MSE n.239/EL-177/141/2011 del 07/04/2011," SINTESI NON TECNICA.

[26] RTE, "Nouvelle interconnexion lectrique souterraine France-Italie," Dossier de presse, 2015, (Last accessed 27/06/2016). [Online]. Available: file:///C:/Users/Alessandro%20Berto/Downloads/20150702_savoie_piemont_dossier_de_presse.pdf

[27] "New strategic interconnection Italy-France for Terna R. I. and RTE," (Last accessed: 26/06/2016). [Online]. Available: http://www.prysmiangroup.com/en/corporate/media/news/New-strategic-interconnection-Italy-France-for-Terna-R.-I.-and-RTE/

[28] "Alstom to build HVDC VSC converter stations for the France-Italy transmission link," Press Center, Sep. 2015, (Last accessed: 27/06/2016). [Online]. Available: http://www.alstom.com/press-centre/2015/9/alstom-to-build-hvdc-vsc-converter-stations-for-the-france-italy-transmission-link/

[29] "HVDC Projects listing, prepared for the HVDC and flexible AC transmission subcommittee of the IEEE transmission and distribution committee," 2013, (Last accessed: 16/04/2016). [Online]. Available: http://www.ece.uidaho.edu/hvdcfacts/

[30] ABB, "North-East Agra. Will supply electricity to serve 90 million people." (Last accessed: 21/03/2016). [Online]. Available: http://new.abb.com/systems/hvdc/references/north-east-agra

[31] W. Leterme, P. Tielens, S. De Boeck, and D. Van Hertem, "Overview of grounding and configuration options for meshed HVDC grids," *IEEE Trans. Power Delivery*, vol. 29, no. 6, pp. 2467–2475, 2014.

[32] A. Egea-Alvarez, J. Beerten, D. Van Hertem, and O. Gomis-Bellmunt, "Primary and secondary power control of multiterminal HVDC grids," in *10th IET International Conference on AC and DC Power Transmission (ACDC 2012),*. Birmingham, 4-5 Dec. 2012, pp. 1–6.

[33] J. Beerten, D. Van Hertem, and R. Belmans, "VSC MTDC systems with a distributed DC voltage control - A power flow approach," in *IEEE PowerTech,*. Trondheim, 19-23 June 2011, pp. 1–6.

[34] T. M. Haileselassie and K. Uhlen, "Primary frequency control of remote grids connected by multi-terminal HVDC," in *Power and Energy Society General Meeting,*. Minneapolis, (MN), 25-29 July 2010, pp. 1–6.

[35] A. Bayo Salas, "Operation, control and optimization of a meshed-HVDC system," Master's thesis, Universitat Politècnica de Catalunya, 2013.

[36] S. Cole and R. Belmans, "A proposal for standard VSC HVDC dynamic models in power system stability studies," *Electr. Power Syst. Res.*, vol. 81, no. 4, pp. 967–973, Apr. 2011.

[37] A. Egea-Alvarez, A. Junyent-Ferré, and O. Gomis-Bellmunt, "Active and reactive power control of grid connected distributed generation systems," in *Modeling and control of sustainable power systems*. Springer, 2012, pp. 47–81.

[38] N. Mohan and T. M. Undeland, *Power electronics: converters, applications, and design*. united States of America, John Wiley & Sons, 2007.

[39] J. Arrillaga, Y. H. Liu, N. R. Watson, and N. J. Murray, *Self-commutating converters for high power applications*. Singapore, John Wiley & Sons, 2010.

[40] A. Yazdani and R. Iravani, *Voltage-sourced converters in power systems: modeling, control, and applications*. United States of America, John Wiley & Sons, 2010.

[41] M. C. Chandorkar, D. M. Divan, and R. Adapa, "Control of parallel connected inverters in standalone AC supply systems," *IEEE Trans. Ind. Appl.*, vol. 29, no. 1, pp. 136–143, Jan.-Feb. 1993.

[42] A. Bergen, *Power systems analysis*. Old Tappan, NJ, Prentice Hall, Inc.,, 1986.

[43] M. P. Kazmierkowski and L. Malesani, "Current control techniques for three-phase voltage-source PWM converters: a survey," *IEEE Trans. Ind. Electron.*, vol. 45, no. 5, pp. 691–703, Oct. 1998.

[44] R. H. Park, "Two-reaction theory of synchronous machines generalized method of analysis-part I," *Trans. Am. Inst. Electr. Eng.*, vol. 48, no. 3, pp. 716–727, Jul. 1929.

[45] D. H. Wolaver, *Phase-locked loop circuit design*. Englewood Cliffs, New Jersey, Prentice-Hall, 1991.

[46] G.-C. Hsieh and J. C. Hung, "Phase-locked loop techniques. A survey," *IEEE Trans. Ind. Electron.*, vol. 43, no. 6, pp. 609–615, Dec. 1996.

[47] V. Kaura and V. Blasko, "Operation of a phase locked loop system under distorted utility conditions," in *Eleventh Annual Applied Power Electronics Conference and Exposition, APEC'96.*, vol. 2. San Jose, (CA), 3-7 Mar 1996, pp. 703–708.

[48] C. D. Schauder and R. Caddy, "Current control of voltage-source inverters for fast four-quadrant drive performance," *IEEE Trans. Ind. Appl.*, vol. 2, no. IA-18, pp. 163–171, 1982.

[49] C. Schauder and H. Mehta, "Vector analysis and control of advanced static VAR compensators," in *Generation, Transmission and Distribution, IEE Proceedings*, vol. 140, no. 4. IET, Jul. 1993, pp. 299–306.

[50] M. Bisiacco and M. E. Valcher, *Controlli automatici*. Padova, Libreria Progetto, 2008.

[51] C. Bajracharya, M. Molinas, J. A. Suul, T. M. Undeland *et al.*, "Understanding of tuning techniques of converter controllers for VSC-HVDC," in *Nordic Workshop on Power and Industrial Electronics (NORPIE/2008),*. Helsinki University of Technology, Espoo, Finland, June 9-11, 2008.

[52] A. J. Beddard, "Factors affecting the reliability of VSC-HVDC for the connection of offshore windfarms," Ph.D. dissertation, The University of Manchester, Manchester, UK, 2014.

[53] J. Beerten, S. DArco, and J. Are Suul, "Frequency-dependent cable modelling for small-signal stability analysis of VSC HVDC systems," IET Generation, Transmission & Distribution, in press (available online).

[54] A. Hammad, "Stability and control of HVDC and AC transmissions in parallel," *IEEE Trans. Power Delivery*, vol. 14, no. 4, pp. 1545–1554, Oct. 1999.

[55] K. To, A. David, and A. Hammad, "A robust co-ordinated control scheme for HVDC transmission with parallel AC systems," *IEEE Trans. Power Delivery*, vol. 9, no. 3, pp. 1710–1716, Jul. 1994.

[56] N. Vovos and G. Galanos, "Enhancement of the transient stability of integrated AC/DC systems using active and reactive power modulation," *IEEE Power Eng. Rev.*, vol. PER-5, no. 7, pp. 33–34, Jul. 1985.

[57] N. R. Chaudhuri and B. Chaudhuri, "Adaptive droop control for effective power sharing in multi-terminal DC (MTDC) grids," *IEEE Trans. Power Syst.*, vol. 28, no. 1, pp. 21–29, 2013.

[58] R. Eriksson, J. Beerten, M. Ghandhari, and R. Belmans, "Optimizing DC voltage droop settings for AC/DC system interactions," *IEEE Transactions on Power Systems*, vol. 29, no. 1, pp. 362–369, 2014.

[59] J. Beerten, R. Eriksson, and R. Belmans, "Influence of DC voltage droop settings on AC system stability," in *10th IET International Conference on AC and DC Power Transmission (ACDC 2012)*. Birmingham, 4-5 Dec. 2012, pp. 1–5.

[60] E. Prieto-Araujo, F. D. Bianchi, A. Junyent-Ferre, and O. Gomis-Bellmunt, "Methodology for droop control dynamic analysis of multiterminal VSC-HVDC grids for offshore wind farms," *IEEE Trans. Power Delivery*, vol. 26, no. 4, pp. 2476–2485, Oct. 2011.

[61] M. Aragüés-Peñalba, A. Egea-Àlvarez, O. Gomis-Bellmunt, and A. Sumper, "Optimum voltage control for loss minimization in HVDC multi-terminal transmission systems for large offshore wind farms," *Electr. Power Syst. Res.*, vol. 89, pp. 54–63, aug 2012.

[62] R. Wiget and G. Andersson, "Optimal power flow for combined AC and multi-terminal HVDC grids based on VSC converters," in *IEEE Power and Energy Society General Meeting*. San Diego, (CA), 22-26 July 2012, pp. 1–8.

[63] F. D. Bianchi and O. Gomis-Bellmunt, "Droop control design for multi-terminal VSC-HVDC grids based on LMI optimization," in *50th IEEE Conference on Decision and Control and European Control Conference (CDC-ECC),*. Orlando, (FL), 12-15 Dec. 2011, pp. 4823–4828.

[64] J. Beerten and R. Belmans, "Analysis of power sharing and voltage deviations in droop-controlled DC grids," *IEEE Trans. Power Syst.*, vol. 28, no. 4, pp. 4588–4597, 2013.

[65] G. Kron, *Tensor analysis of networks*. New York, J. Wiley & Sons, 1939.

[66] ABB, "It is time to connect - technical description of HVDC Light technology," Technical Report, Mar. 2008.

[67] S. Cole, J. Beerten, and R. Belmans, "Generalized dynamic VSC MTDC model for power system stability studies," *IEEE Trans. Power Syst.*, vol. 25, no. 3, pp. 1655–1662, Aug. 2010.

Appendix A

Power flow calculation

This appendix contains the mathematical description of the steady-state power flows in the DC grid that can be also found in [67]. To initialize the simulations performed in the thesis, the voltage, current and power at each terminal of the bipolar grid have been calculated with the following method.

The steady-state equations of the DC network are

$$\mathsf{Y}_{\mathsf{DC}}\mathbf{U_{DC}} = \mathbf{I_{DC}} \tag{A.1}$$

$$P_{DCi} = 2I_{DCi}U_{DCi} \qquad \forall i \leq n \tag{A.2}$$

where Y_{DC} is the admittance matrix of the DC network, $\mathbf{U_{DC}}$ the vector of the node voltages, $\mathbf{I_{DC}}$ the vector of the currents injected by the converters and n the number of converters in the grid. Since the equation describe a steady-state operation, the admittance matrix contains only line resistances. Furthermore, the initial mode is balanced and thus no current is flowing in the return path. In the admittance matrix, a zero entry can substitute the metallic return resistance. Alternatively, the power flow calculation can be undertaken only for one pole. In balanced mode, the other pole has exactly the same magnitude for node voltages and currents, but reversed sign.

Equation (A.2) is substituted in (A.1) to obtain a system of non linear equations

$$0 = \mathsf{Y}_{\mathsf{DC}}\mathbf{U_{DC}} - \left[\frac{P_{DCi}}{2U_{DCi}}\right]. \tag{A.3}$$

In oder to find a steady-state starting point for the simulations, the centralized control logic is hipotetically applied (it might not correspond with the actual (dynamic) control strategy). As a converter controls the voltage (the last converter in the following formulas) and the others control the power, the vector of unknowns is

$$\mathbf{X} = \left(\frac{\mathbf{X_1}}{X_2}\right) = \begin{pmatrix} U_{DC_1} \\ \vdots \\ \frac{U_{DC_{n-1}}}{P_{DC_n}} \end{pmatrix} \tag{A.4}$$

The admittance matrix is partitioned in the following way

$$\left(\begin{array}{c|c} \mathsf{Y}_{11} & \mathbf{Y_{12}} \\ \hline \mathbf{Y_{21}} & y_{22} \end{array}\right) \tag{A.5}$$

where Y_{11} is a matrix of dimension $(n-1)\times(n-1)$, $\mathbf{Y_{12}}$ and $\mathbf{Y_{21}}$ are respectively a column and a row of length $(n-1)$ and y_{22} is a scalar. The Newton method can be now applied to solve in an iterative manner the system

$$\begin{cases} 0 = \mathsf{Y}_{11}\mathbf{X_1} + \mathbf{Y_{12}}u_{DCeref} - (P_{DCi}/2X_{1i}) \\ 0 = \mathsf{Y}_{21}\mathbf{X_1} + \mathbf{y_{22}}u_{DCeref} - (X_2/2u_{DCeref}) \end{cases} \tag{A.6}$$

where u_{DCref} is the value of the reference voltage in the slack bus controller.

Finally, DC currents injected by the converters are found solving equation (A.1) and DC power substituting voltages and currents in the network equation (A.2). These results are used to initialise the droop control laws.

Appendix B

Per unit conversion

In this appendix the per unit conversion used in the thesis is defined. The base values of power and voltage are

$$P_b = U_n I_n \sqrt{3} \tag{B.1}$$

$$U_b = U_n \sqrt{\frac{2}{3}}. \tag{B.2}$$

The subscripts n and b indicates respectively the nominal values and the per unit base values. The per unit base values of current and impedance are

$$I_b = I_n \sqrt{2} \tag{B.3}$$

$$Z_b = \frac{U_b}{I_b} = \frac{3}{2}\frac{U_b^2}{S_b}, \tag{B.4}$$

while base resistance, inductance and capacitance are

$$R_b = Z_b \tag{B.5}$$

$$L_b = \frac{Z_b}{\omega_b} \tag{B.6}$$

$$C_b = \frac{1}{Z_b \omega_b} \tag{B.7}$$

where ω_b is defined equal to the pulsation at the frequency of 50 Hz. With this per unit definition, the power at one terminal of a monopolar configuration is

$$P_{DC_b} = U_{DC_b} I_{DC_b}, \tag{B.8}$$

while for a bipolar configuration

$$P_{DC_b} = 2 U_{DC_b} I_{DC_b}. \tag{B.9}$$